2004

Estimation of weather impacts on distribution-transformer energy losses

Mengsteab Habtegiorgis Weldegaber
San Jose State University

ESTIMATION OF WEATHER IMPACTS ON DISTRIBUTION-TRANSFORMER ENERGY LOSSES

A Thesis

Presented to

The Faculty of the Department of Meteorology

San Jose State University

In Partial Fulfillment

of the Requirement for the Degree

Master of Science

By

Mengsteab Habtegiorgis Weldegaber

August 2004

APPROVED FOR THE DEPARTMENT OF METEOROLOGY

R. Bornstein

Prof. Robert Bornstein

Eugene Cordero

Prof. Eugene Cordero

Robert Van Buskirk

Dr. Robert Van Buskirk

APPROVED FOR THE UNIVERSITY

Pamela C Stark

ABSTRACT

ESTIMATION OF WEATHER IMPACTS ON DISTRIBUTION-TRANSFORMER ENERGY LOSSES

By

Mengsteab Habtegiorgis Weldegaber

Current U.S. Department of Energy (DOE) estimates of electrical distribution-transformer (DT) energy-losses do not incorporate weather effects. While the industry-standard Institute of Electrical and Electronics Engineers (IEEE) model only includes ambient temperature impacts, it excludes wind and solar heating effects, which may significantly alter DT energy losses. In the current study, the IEEE model is modified to incorporate these effects, and results are compared for a variety of DTs sample in several climatic regions. Results show that DT temperatures, fluxes, and aging rates are dependent on weather impacts, with specific impacts dependent on climate regime. Resulting estimates of weather impacts on DT energy losses will be used by DOE to evaluate the errors that result from ignoring weather impacts.

To the memory of

my brother

Tesheme Habtegiorgis Weldegaber

Acknowledgements

I would like to thank to my advisor, Dr. Robert Bornstein of San Jose State University (SJSU), for the tremendous assistance and guidance he provided to me during this research. I also want to thank Dr. Robert Van Buskirk of Lawrence Berkeley National Laboratory for the generous financial support for my graduate tuition through the Eritrean Technical Exchange Program. I also want to thank him for his invaluable assistance in computer programming and for the wealth of knowledge and experience he shared with me during this effort. I would also like to thank Dr. Eugene Cordero of SJSU for being a member of my thesis committee.

The research was funded by of the Lawrence Berkeley National Laboratory (LBNL). Grateful appreciation is extended to the Environmental Energy Technologies Division of LBNL for providing the input data used in the study.

Finally, I wish to extend thanks to my friends and colleagues in the Meteorology Department at SJSU, with whom I spent most of my time in three years of study.

TABLE OF CONTENTS

List of Tables

(Note that Tables are found at end of thesis)

List of Figures

(Note that Figures are found after Appendix A)

List of Figures (continued)

List of Figures (continued)

1. Introduction

Distribution transformers (DTs) transfer electrical energy from primary distribution circuits to secondary or to consumer service circuits. Virtually all US electrical power passes through one or more DTs. Liquid-immersed DTs, which typically use mineral oil as a combination coolant and dielectric medium, are normally used outdoors. Electric utilities operate about 90% of all liquid-immersed transformers (Barnes et al. 1994, 1995). Dry-type DTs are air-cooled and are used mostly by commercial and industrial customers.

Of the 1999 US electrical energy generation of 3.7×10^{12} kWh (EIA 2002a), about 7.5% was lost to heat. Sixty five percent of this is transmission loss, and 41% (7.4×10^{10} kWh) of that is associated with DTs. Despite their high (>99%) efficiencies (Beaumont 1988), with total US 1999 retail electricity revenues at $217 billion (EIA 2002b), DT losses were thus $4 billion due to continuous normal operation. Environmental considerations and rising energy costs have produced strict requirements for transformer efficiency (Harrison 1988, Holland 1992).

The US Department of Energy (DOE) is currently involved in setting feasible DT efficiency standards (Barnes et al. 1995), i.e., benefits must outweigh burdens. Costs-benefits calculations depend on accurate

estimates of DT losses, which vary with DT temperature (dependent on design), electrical-load variation, and ambient weather conditions. DTs are rated by their electrical-load capacity, expressed in terms of their "rated" (or name-plate) power rating.

Electrical power can be expressed as i^2R (where all symbols are defined in Appendix A), but as voltage V equals iR, it can also be expressed as Vi. In alternating current (ac) circuits, the actual power delivered also depends on voltage phases and current waveform. If voltage and current are in phase, then apparent power (in kilo-volt-amperes, kVA) is equal to actual load (in kilowatts). The kVA rating of any DT is thus the load it can continuously carry without its average internal winding temperature exceeding ambient air temperature by more than a specified design amount.

Peak losses generally occur during hot days, when air conditioning demand is high; power demand surges (and electricity costs thus rise); equipment overloads, overheats, and fails; and power outages result. Current mineral-oil transformer ratings, however, use only a 24 h average standard ambient temperature of 30°C (IEEE 1995).

In 1996, the National Electric Manufacturers Association (NEMA) developed the voluntary energy DT efficiency standard NEMA TP 1-1996

(NEMA 1996). It allows short payback periods to recover the additional costs mandated by the more efficient DTs from money saved by resulting reduced energy consumption. It describes minimum transformer efficiencies for 73 liquid-immersed and dry-type DTs. It also describes total owning cost methodologies for these DTs, based on kVA rating. The NEMA standard TP-1 reference load for liquid-immersed DTs (50% of nameplate capacity) appears higher than for typical utility applications. One hundred percent compliance with the voluntary NEMA minimum efficiency standard could save about 7.3×10^{11} kWh of primary energy during the 30-year period from 2004 (Barnes et al. 1997).

Various DT heat-loss mathematical models exist to describe heat transfer and fluid-flow phenomena in liquid-immersed DTs during transient loading (Fig. 1). One of the first (Cooney 1925) found exponential average oil (T_0) and winding (T_w) temperature-rises above ambient-air values (T_a) in self-cooled oil-immersed DTs. Comparison of predicted and observed total final rises ($\Delta T_{wa} = \Delta T_{wo}+\Delta T_{oa}$) showed generally good agreement.

Vogel and Narbutovskih (1942) extended the analysis to include a new equation to determine the maximum "safe" T_w value, i.e., the "hot-spot" temperature T_h. Based on an "aging" study and model results, they recommended that short-term peak T_h values should not exceed its aver-

age value by more than 10°C. A simplified graphical method (on special transient-coordinate paper) for computation of DT temperature-rises was developed by Narbutovskih (1947). It is based on exponential solutions for thermal-transient time-constants dependent on a linear proportionality between hot-surface heat-dissipation rate and temperature-rise.

Testing was begun in 1957 (Acker 1976) to evaluate the lifetime of 55°C average winding-rise insulation DT systems. A safety factor of five on max temperature rise was applied to the most pessimistic results to obtain an average DT-life of 20 years, a value long used in many loading guides. This includes 180 000 h at a T_h value of 95°C, a value also used as the standard for many years. Recent tests by DT manufacturers on 65°C average winding-rise insulation systems have, however, demonstrated a similar useful life at a T_h value of 110°C (IEEE 1995). Functional tests and service experience even suggest a reasonable DT life of 15-20 years at a T_h value of 110°C. A limit of 140°C has been proposed (IEEE 1981), although T_h values of up to 180°C during emergency overloads are allowed by the Institute of Electrical and Electronics Engineers (IEEE) loading guide (Pierce 1994).

Theoretical and experimental studies of heated cylinders in cross flows found cylinder height-to-diameter ratio as the most important body property for determination of convective heat losses (Ghisalberti and

Kondjoyan 1999). Based on data from several hundred experiments, a relationship between Reynolds number (Re) and convective heat loss was proposed by Zukauskas (1972) for $Re < 10^6$. Additional experiments by Morgan (1975), however, showed a different relationship for $7x10^4 < Re < 10^6$. Later experimental evidence by Quarmby and Al-Fakhri (1980) resolved the disagreement in favor of Zukauskas.

The IEEE (1981) model, herein called IEEE81, contained a T_h predictor equation that included a vertical gradient of T_o to define an "above the windings" oil temperature T_T. It also used an exponential expression with a time constant (dependent on changing input load) to determine a steady-state oil-duct temperature T_D. Hot-spot winding temperature T_h is thus the sum of the: (1) assumed constant T_a, (2) top-oil temperature-rise over ΔT_a, and (3) hot-spot winding-temperature rise over ΔT_T.

An experimental study of the low-temperature behavior of paraffinic DT-oil by Aubin and Langhame (1992) overcame the previous 0°C T_a-limit in the widely used American National Institute of Standards (ANSI) DT model. Their new Institut de Recherche d'Hydrio-Quebec (IREQ) model was thus valid down to –40°C, as it accounted for variations in physical oil-characteristics, such as viscosity, T_a-induced cooling, and thermal load (as a function of changes in copper resistance).

Results showed that during overload periods, T_D rises rapidly with a time constant equal to the winding time-constant.

Pierce (1992) showed that during overload-periods, IEEE81 produces T_D values higher than T_T values, resulting in under-predicted T_h values. They thus incorporated the IREQ insights and interior DT fluid-flow conditions into IEEE81, to produce the IEEE95 (1995). The new model thus considers: 65°C mineral-oil coolants; different cooling mode options; winding duct oil temperature rise (ΔT_{DB}); resistance and viscosity changes; and T_a changes during a load-cycle. IEEE95 thus produced more accurate predicted DT loading–capacities, based on limits on predicted T_T and T_h values.

While the IEEE95 model was developed to estimate DT temperatures and their effects on DT heat loss, it assumes a fixed ambient air temperature and it ignores wind and solar-heating effects. Its use in current DOE efficiency standard setting processes is thus limited, as solar radiation and wind conditions may significantly alter DT losses and their time variations. The current effort thus modifies the IEEE95 model to calculate DT energy losses resulting from wind and solar radiation impacts in a variety of climate types over a range of DT designs and loads.

2. Methodology

A series of simulations are thus carried out to investigate weather impacts on DT heat losses and efficiency. Simulations are carried out for cities in different US climatic regions with different DT kVA rating (sizes) and cooling modes. This study only considers the simple case where DT voltage and current are in phase.

A. DT design

Electric power from a power plant is transferred to end-users by utility transmission and distribution systems through a network of power lines and associated components. These include DTs to convert high-voltage electricity from a primary distribution circuit to lower-voltage electricity for the secondary distribution circuits in homes and businesses. DTs consist of three basic elements: primary winding, secondary winding, and core.

Windings are wire coils around a core of high-magnetic material. The primary winding is connected to an electric source, while the secondary winding is connected to an output or load (Barnes et al. 1996). The core may be of silicon steel or another magnetic material (such as amorphous metal) and it provides a path for the magnetic flux that links the windings. An alternating flux is established in the core when the prim-

ary winding is connected to an ac voltage source. Its strength is proportional to the ratio of the number of turns in two windings. An ideal DT has no losses or leakage flux, and the ratio of voltages induced in the two windings is equal to the ratio of the number of turns in each.

As ideal DTs neither store nor lose energy, the power input to the primary windings must equal that output to the secondary windings. As primary power input is the product of voltage and current, secondary power output must also equal this product. This implies that the ratio of the primary and secondary currents is also inversely proportional to turn ratio.

While modern DTs approach the ideal, losses do exist (Barnes et al. 1996), as voltage drops through a DT under load conditions. Voltage ratio is thus not exactly equal to turn ratio, and excitation currents flow in DTs even with no external current. Losses at load are directly proportional to the product of the current squared and effective winding resistance (the latter is influenced by temperature) (Montsinger 1930).

No-load losses include dielectric, conductor (due to excitation and circulation currents), and core (dominant one) losses. Core loss is associated with the time-varying magnetizing force, and results from hysteresis and eddy-currents in the core. Dependent upon excitation voltage,

they may increase sharply if rated DT voltage is exceeded, with an inverse dependence on core temperature.

Losses associated with carrying loads are referred to as load losses. Unlike no-load losses, load losses vary with the square of DT load current and include: (1) resistive heating (I^2R) losses in windings due to load and to eddy currents (major DT loss), (2) stray loss due to leakage fluxes in windings, core clamps, etc., and (3) loss due to circulating currents in parallel winding strands. As load losses vary with the square of load current, DT efficiency is load-dependent (Barnes et al. 1996, Feinberg 1979). Time variations of each of these energy sources and losses must be accounted for in realistic DT energy-efficiency models.

B. Models

1) IEEE95

IEEE95 accommodates four radiator cooling-modes:

- OA: Natural-convection oil-flow through windings and radiators; and natural-convention air flow over tanks and radiators.
- FA: Natural-convection oil-flow through windings and radiators; and forced-convection (by fans) air-flow over radiators.

- DFOA: Forced oil-flow through windings and radiators (or heat exchangers) by pumps; oil directed from radiators (or heat exchangers) into windings; and air forced over radiators (or heat exchangers) by fans.

- NDFOA: Forced oil-flow through radiators by pumps; oil forced to flow into tank by pumps, thus bypassing windings; and air forced over radiators (or heat exchangers) by fans.

For natural circulation (OA, FA, and DFOA) modes under steady state conditions, oil temperatures at the winding-duct exit T_D and in the top oil T_T are assumed equal. NDFOA mode $T_D > T_T$, as the latter has bypassed the hot windings.

IEEE95 calculates (as shown below) the following eight transient internal DT temperatures from conservation of energy equations (Fig. 1): winding T_W, hot spot (max winding) T_h, transformer-oil T_o, hot spot oil T_p, top oil T_T, cooling duct oil T_d, top-duct oil T_D, and bottom oil T_B. It also calculates the following DT heat fluxes: winding generation Q_w^+, core loss Q_c^+, stray loss Q_s^+, total loss Q_A^+, hot-spot generation Q_h^+, winding absorption Q_{aw}, hot-spot absorption Q_{ah}, oil absorption Q_{ao}, winding loss Q_w^-, hot-spot loss Q_h^-, and oil loss Q_o^-.

DT overload, and DT-insulation deterioration, is limited by the hot-spot winding temperature T_h (Montsinger and Ketchum 1942), which has the following components:

$$T_h = T_a + \Delta T_{Ba} + \Delta T_{pB} + \Delta T_{hp}\,, \tag{1}$$

or in expanded form

$$T_h = T_a + (T_B - T_a) + (T_P - T_B) + (T_h - T_p)\,. \tag{2}$$

The above relationships are modified during overload conditions, when $T_D < T_T$ and when $\Delta T_{PB} = T_d - T_B)$ to $\Delta T_{hp} = \Delta T_{Ba}$.

From conservation of energy, internal heat generated by windings Q_w^+ in time Δt is absorbed by the windings as Q_{aw} or lost by them as Q_w^-, i.e.,

$$\frac{dQ_w^+}{dt} = \frac{d(Q_{aw} + Q_w^-)}{dt}\,. \tag{3}$$

Winding heat-generation Q_w^+ is

$$Q_w^+ = L^2 \left\{ P_w \cdot \gamma_w + \frac{Pe}{\gamma_w} \right\} \Delta t\,, \tag{4}$$

where fractional rated hourly-load L is an input parameter.

The temperature correction (due to resistance change) for winding losses γ_w is given by:

$$\gamma_w = \frac{(T_w + T_k)}{(\tilde{T}_w + T_k)} \quad . \tag{5}$$

The first term on the right hand side (RHS) of Eq. (4) represents the corrected internal-winding heat-production rate due to electric current within windings, while the second represents the corrected internal winding eddy-current heat-loss rate. Heat-losses P_w and P_e are input parameters.

Winding loss Q_w^- in Eq. (3) for cooling modes OA, FA, and NDFOA is

$$Q_w^- = \zeta_w (P_w + P_e) \Delta t \cdot \mu_w' \, . \tag{6}$$

Fluid viscosity μ_w' is corrected for temperature via

$$\mu_w' = \left\{ \zeta_w \frac{\tilde{\mu}_w}{\mu_w} \right\}^{1/4} \tag{7}$$

$$\zeta_w = \frac{(T_w - T_d)}{(\tilde{T}_w - \tilde{T}_d)} \quad , \tag{8}$$

where the relationship between μ and T is

$$\mu = B \exp^{F/(T+273)} . \tag{9}$$

All rated quantities $(\tilde{})$ are input parameters. For the DFOA mode, no correction is needed, i.e.,

$$\mu'_w = 1 . \tag{10}$$

Heat absorbed Q_{aw} by windings in Eq. (3) is given by

$$Q_{aw} = C \Delta T_w , \tag{11}$$

where

$$C = (mc)_w = \frac{\tau_w (P_w + P_e)}{(\tilde{T}_w - \tilde{T}_d)} , \tag{12}$$

and where input winding time constant τ_w is determined from testing-derived cooling-curves.

Substitution of Eq. (11) into the finite difference form of (3) yields

$$\frac{T_w^{n+1} - T_w^n}{\Delta t} = \frac{Q_w^{+\,n} - Q_w^{-\,n}}{C \Delta t} , \tag{13}$$

while insertion of Eqs. (4) and (6) into (13) yields the final predictive equation for T_W

$$T_w^{n+1} = T_w^n + \frac{(\tilde{T}_w - \tilde{T}_d)}{\tau_w (P_w + P_e)} \left\{ L^2 \left(P_w \gamma_w + \frac{P_e}{\gamma_w} \right) - \frac{(\tilde{T}_w - \tilde{T}_d) \zeta_w \cdot \mu'_w}{\tau_w} \right\}. \quad (14)$$

Winding duct oil temperature rise ΔT_{DB} is determined from:

$$\Delta T_{DB} = T_D - T_B = \left\{ \frac{Q_W^-}{(P_W + P_e)\Delta t} \right\}^x (\tilde{T}_D - \tilde{T}_B), \quad (15)$$

and average cooling-duct oil temperature T_d is defined as

$$T_d = \frac{T_D + T_B}{2}. \quad (16)$$

For the NDFOA cooling mode, if the rated-load duct oil temperature $\tilde{T}_D$ is unknown, it is assumed equal to $\tilde{T}_W$ (Pierce 1992).

"Hot-spot" oil temperature T_p is normally given by

$$T_p = T_B + (T_D - T_B).h, \quad (17)$$

but when $T_p < T_D$, it is assumed equal to T_D, as the upper portion of the winding is in contact with the hotter top-oil.

From energy conservation, internal heat generated Q_h^+ at the location of T_h over Δt is again absorbed as Q_{ah} or lost as Q_h^-, i.e.,

$$\frac{dQ_h^+}{dt} = \frac{d(Q_{ah} + Q_h^-)}{dt} \quad . \tag{18}$$

To account for the additional hot-spot heat generation, the heat loss at the average winding temperature P_W becomes:

$$P_h = \left(\frac{\tilde{T}_h + T_k}{\tilde{T}_w + T_k} \right) P_w \cdot \tag{19}$$

Internal heat generation Q_h^+ is thus calculated from

$$Q_h^+ = L^2 \left\{ P_h \cdot \gamma_h + \frac{P_{eh}}{\gamma_h} \right\} \Delta t \quad , \tag{20}$$

where

$$P_{eh} = E_h \cdot P_h \tag{21}$$

$$\gamma_h = \frac{(T_h + T_k)}{(\tilde{T}_h + \tilde{T}_k)} \quad . \tag{22}$$

The first term on the RHS of Eq. (20) represents internal winding heat production rate at the location of T_h due to winding loss (corrected

by a resistance-change temperature factor). The second represents the internal winding heat production rate at the location of T_h due to eddy-current heat loss (corrected by a temperature factor).

The corresponding hot-spot heat loss Q_h^- for cooling modes OA, FA, and NDFOA is given by

$$Q_h^- = \chi_h \cdot \mu_h'(P_h + P_{eh})\Delta t, \tag{23}$$

where

$$\mu_h' = \left\{\frac{(T_h - T_p)\tilde{\mu}_h}{(\tilde{T}_h - \tilde{T}_p)\mu_h}\right\}^{1/4} \tag{24}$$

$$\chi_h = \frac{(T_h - T_p)}{(\tilde{T}_h - \tilde{T}_p)} \cdot \tag{25}$$

For the DFOA cooling mode, oil is pumped and a viscosity correction is again not required, i.e., $\mu'_h = 1$.

Hot-spot heat absorption Q_{ah} is given by

$$Q_{ah} = C\ \Delta T_h \cdot \tag{26}$$

Substitution of Eq. (26) into the finite difference form of (18) yields

$$\frac{T_h^{n+1} - T_h^n}{\Delta t} = \frac{Q_h^{+n} - Q_h^{-n}}{C\Delta t}, \tag{27}$$

and substitution of Eqs. (20) and (23) into (27) yields the following predictive equation for T_h

$$T_h^{n+1} = T_h^n + \frac{1}{C}\left\{ L^2\left(P_h\gamma_h + \frac{P_{eh}}{\gamma_h}\right) - \chi_h \cdot \mu'_h (P_h + P_{eh}) \right\}. \qquad (28)$$

Determination of T_o is similar to that for T_w, as it involves three heat losses by the: windings Q_w^- to duct oil, core Q_c^+, and stray losses Q_s^+. The heat is then either absorbed by main-tank oil and radiator coolants as Q_{ao} or lost to the ambient air by the radiators as Q_o^-. The heat balance equation is thus

$$\frac{d(Q_w^- + Q_c^+ + Q_s^+)}{dt} = \frac{d(Q_{ao} + Q_o^-)}{dt} , \qquad (29)$$

with Q_w^- given by Eq. (6). While Q_c^+ varies slightly with T_w, it is herein assumed constant as

$$Q_c^+ = P_c \Delta t , \qquad (30a)$$

With excessive DT-core heat-generation, it is increased to an "over-excitation" value given by

$$Q_c^+ = P_{cx} \Delta t . \qquad (30b)$$

With heat generation by stray losses Q_S^+ given by

$$Q_S^+ = \frac{L^2 \cdot P_S \cdot \Delta t}{\gamma_W} \quad . \tag{31}$$

total internal DT heat generation Q_A^+ is thus given by

$$Q_A^+ = Q_W^+ + Q_c^+ + Q_S^+ \, . \tag{32}$$

Heat loss Q_o^- is a function of T_o-T_a, normalized by the "rated load" loss, i.e.

$$Q_o^- = \left\{ \frac{T_o - T_a}{\tilde{T}_o - \tilde{T}_a} \right\}^{1/y} P_A \cdot \Delta t \, . \tag{33}$$

where P_A is the sum of four input "rated load" component losses:

$$P_A = P_W + P_e + P_S + P_c \quad . \tag{34}$$

The heat absorbed (by tank, core, and oil) Q_{ao} is

$$Q_{ao} = (mc)_A \cdot (\Delta T_o) \quad , \tag{35}$$

where

$$(mc)_A = (mc)_t + (mc)_c + (mc)_o \quad . \tag{36}$$

Substitution of Eqs. (31) and (33)-(36) into the finite difference form of (29) yields

$$\frac{T_O^{n+1}-T_O^n}{\Delta t}=\frac{(Q_W^-+Q_S^++Q_C^+-Q_O^-)}{\Delta t.(mc)_A} \quad , \tag{37}$$

while substitution of Eqs. (4), (30), (31), and (33) into (37) yields the following predictive equation for T_o

$$T_o^{n+1}=T_o^n+\frac{1}{(mc)_A}\left\{\zeta_w(P_w+P_e)\mu'_w+\frac{L^2P_s}{\gamma_w}+P_c-\left(\frac{T_o-T_a}{\tilde{T}_o-\tilde{T}_a}\right)^{1/y}P_A\right\} . \tag{38}$$

Temperature difference ΔT_{TB} is determined in a way similar to ΔT_{DB}, i.e.,

$$\Delta T_{TB}=T_T-T_B=\left\{\frac{Q_o^-}{P_A.\Delta t}\right\}^z.(\tilde{T}_T-\tilde{T}_B), \tag{39}$$

where Q_o^- is given by Eq. (33) and where

$$T_T=T_o+\frac{\Delta T_{TB}}{2} \tag{40}$$

$$T_B=T_o-\frac{\Delta T_{TB}}{2} \quad . \tag{41}$$

Numerical stability conditions (Dusinberre 1961) for the OA, FA, and NDFOA cooling modes show the above system of heat-transfer equations is stable if both the following are satisfied:

$$\frac{\tau}{\Delta t} > \left(\frac{T_w - T_d}{\tilde{T}_w - \tilde{T}_d}\right)^{1/4} \left(\frac{\tilde{\mu}_w}{\mu_w}\right)^{1/4} \tag{42}$$

$$\frac{\tau}{\Delta t} > \left(\frac{T_h - T_p}{\tilde{T}_h - \tilde{T}_p}\right)^{1/4} \left(\frac{\tilde{\mu}_h}{\mu_h}\right)^{1/4}, \tag{43}$$

while for the DFOA cooling mode, only the following must be true:

$$\frac{\tau}{\Delta t} > 1. \tag{44}$$

Functional testing and service experience suggest an average DT lifetime of 15-20 years at a T_h of 110°C. A practical limit on T_h is about 140°C (IEEE 1981), although values up to 180°C during emergency overloads are possible (Pierce 1994).

Winding-insulation deterioration is determined by use of an nondimensional aging acceleration factor A_g. For insulation rated for a 65°C T_h and a 80°C ΔT_{hp} rise, McNutt (1992) gives A_g as:

$$A_g = \exp\left(\frac{15000}{383} - \frac{15000}{(T_h + 273)}\right). \quad (45)$$

For continuous-operation at $T_h > 110^oC$, $A_g > 1$ (accelerated aging), while the converse is true at lower T_h values. For variable load (and hence variable T_h) conditions, the equivalent ageing-time E_A is

$$E_A = \sum A_g \cdot \Delta t \ , \quad (46)$$

while the equivalent ageing acceleration factor A_E is

$$A_E = \frac{\sum A_g \cdot \Delta t}{\sum \Delta t}. \quad (47)$$

High temperatures produce large A_g values, and thus more rapid DT aging. Designed for an E_A of approximately 180 000 h over an average lifetime of 30 years, DTs have average annual aging-times of 6000 h. DTs can occasionally operate at $T_h > 110^oC$ and still achieve normal life-times, as long as A_E is not >1.

2) LBNL03wx

The original IEEE95 model excludes wind and solar heating effects on DT energy losses. Solar-absorption heat-gain and convective heat

loss during windy conditions, however, may significantly alter DT temperatures. In the current study, IEEE95 is thus modified to incorporate these effects to produce the LBNL03wx model. While IEEE95 includes infra red (IR) loss in Q_o^-, atmospheric long-wave radiative effects are not included in either model.

Downward solar radiation reaches the earth surface by direct atmospheric transmission and (to a lesser extent) by downward (diffusive) scattering from gas molecules and aerosols. The first component thus depends on latitude ϕ, hour angle ω, solar declination angle (sea-son) δ (ASHRAE 1985, Joseph 1995), while solar absorption further depends on DT: area, shape, and absorptivity.

The vertical, cylindrical DTs of the current study are assumed to have height H equal to twice their diameter D. Their exposed area A_d (top and vertical surface) is thus:

$$A_d = \frac{\pi D^2}{4} + \pi DH \ , \tag{48}$$

with a resulting absorbed diffusive heat-gain Q_d of

$$Q_d = \alpha \left(\frac{\pi D^2}{4} + \pi DH \right) R_d \, . \tag{49}$$

Direct solar radiation Q_i absorbed on its top plus half its vertical area is thus

$$Q_i = \alpha\left(\frac{\pi D^2 \sin Z}{4} + \pi DH\cos Z\right)R_i, \tag{50}$$

where

$$\cos Z = \sin\phi\,\sin\delta + \cos\phi\,\cos\delta\,\cos\omega \tag{51}$$

$$\omega = 15\,(12 - t) \tag{52}$$

$$\delta = \frac{23.45\sin(360\,(284+N))}{365}\,. \tag{53}$$

Total DT solar-radiation heat gain Q_R^+ is thus

$$Q_R^+ = (Q_i + Q_d)\,. \tag{54}$$

Inclusion of Eqs. (49) and (50) yields

$$Q_R^+ = \alpha\left\{\left(\frac{\pi D^2}{4} + \pi DH\right)R_d + \left(\frac{\pi D^2}{4}\sin Z + \pi DH\cos Z\right)R_i\right\}, \tag{55}$$

which reduces Q_o^- as follows:

$$Q_o^- = \left(\frac{T_o - T_a}{\tilde{T}_o - \tilde{T}_a} \right)^{1/y} \cdot P_A \Delta t - Q_R^+ \Delta t \ . \qquad (56)$$

IEEE95 assumes calm-wind conditions, but wind will significantly change DT heat-losses to the surrounding air, as increased speeds carry away additional heat, driving down DT temperatures (Montsinger et al. 1924). Heat dissipation from an electrical apparatus through conduction and radiation is usually small as compared to dissipation by convection (Skinner and Chubb 1913). DT heat loss by convection during windy conditions Q_u^- is assumed (Kreith and Bohn 1997) as

$$Q_u^- = C_h A (T_o - T_a) = C_h A \Delta T_{oa} \ , \qquad (57)$$

where (in the current application) T_a is set equal to observed 2 m values at off-site National Weather Services (NWS) airport stations. This assumes horizontally homogenous temperature fields and a T_a not influenced by local DT heat losses. The latter assumption is problematic in calm conditions, when the same air remains in contact with a DT for extended periods. In such conditions, however, IR emission still carries away some generated DT heat.

The convective heat transfer coefficient C_h in (57) for an air-cooled cylinder (D/H < 4) is given by the following analytical function of R_e over the range (0.7 – 10.0) x 10^5 (Quarmby and Al-Fakhri 1980):

$$Nu = \frac{C_h D}{\lambda} = 0.123 Re^{0.651} + 0.00416 \left(\frac{D}{H}\right)^{0.85} Re^{0.792} \quad , \tag{58}$$

where

$$Re = \frac{\rho D U}{\mu} . \tag{59}$$

The plot of Eq. (59) in Fig. 2 shows that Re increases (over three orders of magnitude) with U most rapidly for speeds < 4 m s^{-1}, before leveling off. Re also increases with increasing DT rating.

The final expression for C_h is thus

$$Ch = \frac{\lambda}{D} \left\{ 0.123 Re^{0.651} + 0.00416 \left(\frac{D}{H}\right)^{0.85} Re^{0.792} \right\} . \tag{60}$$

A plot of Eq. (60) in Fig. 3 shows that C_h again increases (over one order of magnitude) with U most rapidly for speeds < 6 m s^{-1}, before again leveling off. This coefficient, however, decreases with increasing DT kVA-rating. For low wind speeds (< 2 m s^{-1}), C_h values for all DTs should converge to the calm heat transfer coefficient C_o. Laboratory studies by Krei-

th and Bohn (1997) of energy losses from a 250 kVA DT at equilibrium ΔT_{oa} values produced a C_0 value of 8.95 W m^{-2} K (circle in Fig. 3).

With the substitution of Eq. (60) in (57), the heat loss by convection Q_u^- is

$$Q_u^- = \frac{\lambda A}{D}\left(0.123\,\mathrm{Re}^{0.651} + 0.00416\left(\frac{D}{H}\right)^{0.85}\mathrm{Re}^{0.792}\right)(T_o - T_a). \qquad (61)$$

For windy conditions (including solar radiation effects), Q_o^- must thus be reduced as follows:

$$Q_o^- = \left(\frac{T_o - T_a}{\tilde{T}_o - \tilde{T}_a}\right)^{1/y} \cdot P_A \Delta t - Q_R^+ \Delta t + Q_u^- \Delta t \quad . \qquad (62)$$

LBNL03wx thus sequentially solves the following Eqs.: (4) for Q_W^+, (6) for Q_W^-, (11) for Q_{aw}, (14) for T_W, (15) for T_D, (16) for T_d, (17) for T_p, (20) for Q_h^+, (23) for Q_h^-, (26) for Q_{ah}, (28) for T_h, (30) for Q_c^+, (31) for Q_s^+, (32) for Q_A^+, (35) for Q_{ao}, (38) for T_o, (40) for T_T, (41) for T_B, (55) for Q_R^+, (61) for Q_u^-, and (62) for Q_o^-. For simplicity, output values for

only the following (most important) temperatures and fluxes will be shown: T_h, T_o, Q_A^+, and Q_o^-.

C. Simulation design

The current effort involves simulations with IEEE95 in its original form and then with LBNL03wx, its more advanced version. Specific steps include:

1. Translate IEEE95 code from BASIC to FORTRAN, run new code, and check output against previously published BASIC results

2. Run FORTRAN version of IEEE95 for range of DT designs, loads, and ambient-air temperatures

3. Incorporate wind and solar heating effects to IEEE95 to produce LBNL03wx

4. Redo Step 2 simulations with LBNL03wx

5. Compare results of Steps 2 and 4

6. Run LBNL03wx for representative US sample DTs and climate regions.

Three cities were selected to represent a range of US climate regimes: Boston (BOS) in the cold northeast, Phoenix (PHX) in the sunny southwest, and San Francisco (SFO) in a moderate climate. Each yearlong LBNL03wx simulation investigates impacts from wind and/or solar effects on the most significant DT temperatures (coil T_h and oil T_o) and on the heat generation and loss (Q_A^+ and Q_0^-). Results are presented as diurnal variations of: (a) average day hourly values (from one year of data) and (b) values on the day with maximum hourly winding ("hot-spot") temperature T_h. Resulting hot-spot days were found to occur during the: end of May for PHX, mid-June for BOS, and end of July for SFO.

The simulations use yearlong hourly TMY2 weather data from the National Solar Radiation Data Base (NSRDB) (Marion and Urban 1995). Companion input L values from the yearlong Lawrence Berkeley National Laboratory (LBNL) simulation of electrical-use were also obtained from these data (Fig. 4). Four weather-impact sub-cases were simulated: a) ambient temperature only (old IEEE95), b) ambient temperature and wind, c) ambient temperature and solar radiation, and d) all three parameters (new LBNLO3wx).

Heat-flows (units of W s) were derived over a small time period Δt. Of more physical interest, however, are heat-generation and -loss rates.

Simulated heat flows are thus divided by Δt to obtain heat-generation and -loss rates (in watts) denoted by $\dot{q}_A$ and $\dot{q}_O$ respectively.

The TMY2 dataset, which includes data from 239 US stations, was constructed from short-term data-segments taken from "typical periods" during the 30-year record from 1961-90. Values used in the current study include: (measured or modeled) direct normal R_i and horizontal diffuse R_d solar radiative fluxes, air temperature, and wind speed.

The diurnal variation of annual average-day input wind speeds at all three study sites show expected daytime maxima and nighttime minima (Fig. 5a). The two coastal sites (BOS and SFO) show higher speeds than inland PHX, with maxima during late afternoon hours due to sea breeze influences. Hourly "hot-spot day" speeds at BOS and PHX (Fig. 5b) are more irregular (as expected because they are not averages) than the average-day values, while those at SFO are still smooth due to its stronger afternoon sea breeze.

The diurnal variation of annual average-day input air temperature values at all three study sites show expected daytime maxima and nighttime minima (Fig. 6a). Again also expected, PHX is by far the warmest during all hours, with BOS the coolest. Hourly "hot-spot day" values at PHX (end of May hot-spot day) are even higher (as expected) than its

average-day values and show a smoother patter (Fig. 6b). BOS (mid-June hot-spot day) is now warmer than SFO (end of July hot-spot day), and shows an 1100 LST peak value at the onset of its sea breeze. The ocean waters off of SFO that result from "upwelling" produce T_a values colder than those at BOS (reversed from average-day values). The SFO sea breeze effect is only visible in the relatively flat daytime T_a values.

DOE recognized the impracticability of conducting detailed cost-efficiency analyses for each of the 73 NEMA liquid-immersed and dry-type DTs (DTREA 2001). DOE (2001) thus grouped them into 13 design lines based on similarities in design and construction. The current analysis used one of the most common liquid-immersed DT design from the 13 design lines in four representative sizes (15, 50, 250, and 833 kVA) and the large 28 000 kVA DT used in IEEE95 test case.

Gray-painted cylindrical-shaped DTs with heights twice as large as diameters were assumed, as were copper windings and oil coolants. Characteristics, such as physical size and performance, for the 50 kVA DT were taken from DOE (2001), while 28 000 kVA characteristics came from the IEEE95 test case. A "0.75 scaling rule" was used to estimate performance, dimensions, and losses for the 15, 250, and 833 kVA DTs, based on known input value for 50 kVA DT. The scaling rule is as following: losses for a 250 kVA DT are estimated as $(250/50)^{0.75}$ times los-

ses for a 50 kVA DT. DT input parameters, constants, and exponents are shown in Tables 1-3, respectively.

Annual electric utility loads for the three selected stations were obtained from the hourly-load simulations carried out by LBNL (2002) with the DOE-2.1E model. The model estimated cooling, heating, ventilation, interior lighting, and equipment end-uses by use of TMY2 weather data. It also used previously developed commercial 14 building proto-types from the 1184 buildings listed in CBECS (1995) that used unitary heat pumps as the primary cooling/heating equipment. Hourly input L values for the current application are averages of simulated annual loads for the following sample DTs for each selected city: 31 for SFO, 13 for BOS, and 12 for PHX.

Diurnal variations of annual average-day input normalized L values at all three study sites again show expected daytime maxima and nighttime minima (Fig. 7a), are relatively smooth, and show only small inter-city differences. Daytime hourly "hot-spot day" values (Fig. 7b) are almost doubled (as expected) their average-day values, while nighttime values are closer to average-day values.

Annual-peak-hour fractional-load L_{max} (1.0, by definition) at each site was increased to 1.1, so that the current simulations would have a

similar effect as in the validation case, which used that value for six consecutive hours. These conditions reproduce the industry practice of overloading DTs for short periods (IEEE 1981). Resulting L_{max} spikes at 1600 LST (local standard time for each respective time zone) at PHX, and 2 and 6 h earlier at SFO and BOS, respectively, correspond to the semi-random "turn-on and -off" behavior of building cooling equipment.

3. Results

Results are presented from 16 simulations (Table 4) that investigate effects on DT heat losses and temperatures due to changes in input:

- DT parameters, i.e., kVA rating and cooling mode
- climatic parameters, i.e., ambient air temperature, solar radiation, and wind speed.

A. LBNL03 validation simulation

This 24 h simulation compared DT thermal-performance by use of the FORTRAN-based LBNL03 and BASIC-based IEEE95 models for a large US 28 000 kVA transformer in FA cooling mode for a summer day. Hourly IEEE (1995) input values of T_a and fractional electrical load L (which drives internal DT heat generation) are shown in the first two columns of Table 5 and in Fig. 4. While T_a peaks at 1430 LST, overload conditions are specified during six midday hours, with an L_{max} of 1.1 at 1500 and 1600 LST.

Diurnal variations of the four published IEEE95 predicted DT temperatures (T_h, T_p, T_d, and T_B) are identically matched by those from LBNL03 (Table 5), with all eight predicted LBNL03 temperatures generally sinusoidal (Fig. 8a). As generated heat moves from the DT interior to its ex-

terior, peak temperatures lag L_{max} due to the high thermal inertia of interior DT metallic components and insulating oil. Coil hot-spot T_h and nearby oil temperatures T_p thus both peak after 1600 LST, while bottom oil temperature T_B peaks an hour later.

Predicted LBNL03 DT total interior heat generation rate $\dot{q}_A$ and total heat loss rate to surrounding atmosphere $\dot{q}_O$ (both in W) values are normalized by P_A (also in W) to produce (normalized) $\dot{Q}_A$ and $\dot{Q}_O$ values (Fig. 8b). Both lag L_{max}, with a 2 h delay between the peak $\dot{q}_A$ at 1530 LST and peak $\dot{q}_O$ at 1730 LST, again due to the high DT thermal inertia. Comparison with IEEE95 heat fluxes is not possible, as their values were not published.

The FORTRAN-mode LNBL03 thus exactly replicates all published results from the BASIC-mode IEEE95 model under the no-wind conditions in IEEE95. New simulations were thus carried out by an expanded version of LNBL03 (called LBNL03wx) that also includes both wind and solar radiation effects.

B. LBNL03wx base simulations

A typical US small DT was simulated (250 kVA, FA cooling-mode) in the moderate-climate SFO site. As the critical C_O value is always reached

when Re is $0.7x10^5$, for a 250 kVA DT it is reached when U is 2 m s^{-1}. All speeds less than this value should thus be considered as calm. While this was not considered in the current simulations, most speeds in Fig. 5 are > 2 m s^{-1}.

As diurnal DT average-day interior coil-T_h values (Fig. 9a) show that, relative to the old IEEE95 temperature-only formulation, LBNL03wx values are: (a) increased by solar radiation due to DT warming from surface absorption and (b) decreased by wind due to DT cooling from turbulent heat loss to the atmosphere. For all cases, T_h peaks near 1500 LST, as it is driven by internal heat generation from the load L. On the other hand, T_o (Fig. 9b) peaks at 1700 LST for the two calm cases, but peaks an hour earlier in the two windy cases due to increased DT turbulent heat loss.

During nighttime, wind effects dominate those from solar radiation, as only a small residual persists from previous daytime solar heating. The daytime increase of solar energy causes the T_h values of LBNL03wx to rise up to the corresponding temperature-only values at 0900 LST (Fig. 9a). The early morning T_h values of LBNL03wx are initially low because turbulent heat loss is stronger than solar heating. For the nine daytime hours after 0900 LST both effects approximately cancel, but after 1800 LST turbulent cooling eventually dominates.

Similar differences due to weather effects occur with the average oil T_o values (Fig. 9b). With respect to T_h values, they are smoother and cooler, have smaller diurnal variations, have larger wind and solar effects, and have peak values 2 h later. All of these are expected, given that T_o is also assumed as the DT metallic outer skin-temperature, as it is away from internal-coil heat-sources. With wind and solar effects, the daytime increase of T_o values to their corresponding temperature-only values (at 1300 LST) is 4 h later than the more rapid T_h increase. This lag arises as turbulent heat loss is stronger at the DT skin than at its interior.

These diurnal weather impacts on T_0 are more deeply illustrated by the temperature-difference between the various weather cases (Fig. 10a). The two wind-impact differences-curves (t-tw and ts-tsw) have larger values throughout most of the day than do the two solar-impact curves (ts-t and tsw-tw), while during midday hours the wind- and solar- impact curves have similar values. These effects are expected, given both the lack of nocturnal solar heating and its midday peak. Peak solar-impact differences occur 4-5 h earlier (1500-1600 LST) than do peak wind-impact differences, which occur at the time of peak SFO wind speeds.

The windy solar heating case (curve ts-tsw) has a higher T_o difference than without solar heating (t-tw), as solar heating produces higher temperatures, with thus a greater possibility for turbulent cooling. Wind ef-

fects peak in late afternoon due to sea breeze induced peak speeds, although peak cooling lags the sea breeze because of the high DT thermal inertia.

For solar impacts, the largest temperature change is with the calm-condition case (curve ts-t), because turbulent heat-loss lowers both T_o and the differences between temperatures. Peak T_o difference occurs around 1600 LST, about 4 h after the peak DT heat gain due to solar radiation. Peak temperature differences occur at 1600 LST because when afternoon solar absorption decreases; the extra heat loss from the elevated temperatures becomes bigger than the solar absorption heat gain.

Differences in internal-core T_h between the different weather cases (Fig. 10b) are again similar to T_o differences, except that they are more erratic during midday hours when L is maximum and thus the internal heat source is also maximum. This raises T_h, but resulting outward directed heat fluxes (discussed below) then produce a temporary midday dip in T_h values.

Diurnal average-day temperature gradients between internal T_h and outer skin T_o values for different weather cases (Fig. 11) show: (a) expected (load-driven) large daytime and (low-load) small nighttime internal

gradients and (b) weather effects smaller during low speed and non-solar nighttime hours. During daytime hours, the two solar-driven cases produce larger DT gradients, with the calm-solar case (as expected) producing the largest differences. A possible explanation for this counter-intuitive result is that the higher T_0 values during the solar and/or calm cases in-creases transformer-core resistance. For a given load L, this results in increased internal DT heat production, which thus must overbalance the external solar source and/or reduced calm-case cooling.

The maximum SFO "hot-spot" day (22 July) was, as expected, a month after the summer solstice radiation maximum. Internal T_h values (Fig. 12a) are similar to those for the average-day, except that values are higher and the isolated 1-hr input overload (at time of hottest hourly temperature) produces a concurrent isolated peak. While daytime values are almost 40^0C warmer, nighttime values are only about 8^0C higher.

Hot-spot day external T_o values (Fig. 12b) are similar to average-day results, except that they are (as expected) warmer than the average day T_0 results by about 17 and 4^0C during daytime and nighttime hours, respectively. No overload-produced peak value exists, however, as T_o is not dominated by internal heat sources (as peak-day T_h is), as it is more dominated by external weather effects. The two solar heating cases pro-

duce T_h-T_o difference values only up to a few degrees larger (during morning hours) than the two cases without this effect (Fig. 13), again due to increased DT internal electrical resistance at the higher T_h values.

Average-day diurnal DT fractional heat generation rate $\dot{Q}_A$ (year-long simulation $\dot{q}_A$ results normalized by P_A) (Fig. 14a) is almost insensitive to weather elements, although actual generation rates do increase with solar effects and decrease with wind effects. Maximum values occur during mid-afternoon maximum temperature (and load) periods, with smaller uniform nighttime losses. Solar radiation does slightly increase peak $\dot{Q}_A$ values, consistent with the increased electrical-resistances at higher temperatures discussed above.

Corresponding normalized DT surface heat loss (to the environment) rates $\dot{Q}_o$ (Fig. 14b) differ from $\dot{Q}_A$ rates, as they: (a) are strongly influenced by weather effects (as expected), (b) are not uniform during nighttime hours (especially with solar effects), (c) have strong peaks around sunset, and (d) have minimum and peak values delayed by several hours. The temperature-only case shows the smallest $\dot{Q}_o$ diurnal variation, with a minimum a few hours after sunrise (concurrent with minimum ambient temperatures). Its sunset maximum at about 1900 LST is due both

to the large DT thermal inertia (that retards flow of $\dot{Q}_A$ to surface, where it is lost as $\dot{Q}_0$) and to the then maximum (T_o -T_a) gradient.

Hourly solar and wind variations produce greater hourly $\dot{Q}_0$ variations, e.g., solar heating first (after sunrise) produces an inward directed heat flux that partly counters the outward-directed $\dot{Q}_0$. It then increases the fluax by increasing T_o during afternoon and nocturnal hours, as the large DT thermal inertia retards the loss of stored daytime solar energy (as with urban structures). Minimum $\dot{Q}_0$ values are thus delayed further beyond sunrise in both solar heating cases.

Even more significant changes of $\dot{Q}_0$ result from wind effects, as both windy-case day-and night-time peak values occur 1 h earlier and are more extreme, with a cross-over at the time of the maximum ambient temperature (about 1500 LST). As daytime convective heat loss depends on wind speed, $\dot{Q}_0$ is a maximum concurrent with maximum average-day SFO wind speeds, i.e., during afternoon sea-breeze hours (Fig. 5a). Daytime convection thus speeds up losses, producing an earlier peak and a reduced nocturnal $\dot{Q}_0$ value that can more quickly be overcome by sunrise solar-heating.

Maximum hot-spot-day fractional heat generation/loss rates (Figs. 15 a, b) are similar to the average-day results, except that the: (a) daytime $\dot{Q}_A$ and $\dot{Q}_o$ values are almost doubled (as expected) and (b) assumed afternoon over-load produces expected peak $\dot{Q}_A$ values. While relative wind effects on peak-day $\dot{Q}_o$ (relative to average-day values) are generally reduced (as peak temperatures are associated with near-calm conditions), temperature and solar effects are increased (as peak temperatures are associated with strong solar forcing).

Wind and solar impacts (expressed as differences) on actual average-day internal DT heat generation rates $\dot{q}_A$ (Fig. 16a) shows (as compared to the fractional impacts of Fig. 14a) that windy solar-heating (curve ts-tsw) produces larger daytime differences than without solar heating (t-tw), again due to the electrical-resistance effect discussed above. Peak differences occur around 1500 to 1700 LST, several hours after the peak solar radiation. Solar-impacts are again largest with calm conditions (ts-t), because wind (tsw-tw) lowers DT temperatures due to increased turbulent heat loss, and hence deceased resistances.

Maximum hot-spot-day weather-induced $\dot{q}_A$ differences (Fig. 16b) are similar to the average-day results, except that the daytime values are tripled and the afternoon over-load again produces expected irregular

peak-differences. Irregular values occur as midday load effects again produce temporary low values.

C. Parametric studies

The LBNL03wx model was used in parametric studies to investigate impacts on both DT load-produced heat-generation and internal DT heat dynamics from changes in: DT kVA rating, cooling mode, and climatic regime.

1) kVA rating

LBNL03wx simulations were used to investigate impacts on DT heat-loss rates and temperatures as a function of DT kVA rating. The following four representative smaller US DT sizes at SFO in FA cooling mode were considered: 15, 50, 250, and 883 kVA.

Results show no significant dependence of average-day daytime winding temperature T_h on kVA rating (Fig. 17a), with peak values at 1500 LST (time of peak load) in all cases. During the remaining hours, T_h values are proportional to kVA rating, with nocturnal differences up to 7°C. Nighttime differences result as internal heat-generation increases proportionally to DT volume ($\propto D^3$), while heat loss to the environment increases only as its surface area ($\propto D^2$). The high DT thermal inertia

thus cannot move the additional internal heat in the high kVA cases to the surface fast enough for it to dissipate by convection during normally low-speed nocturnal periods. During high-speed daytime hours, strong convection dissipates almost all generated heat, and thus no significant T_h dependence on DT size exists.

A similar pattern generally occurs with outer-skin oil temperature T_o (Fig. 17b), with a maximum nocturnal difference of about 6°C. Impacts (relative to corresponding T_h values) include: (a) nighttime (minimum) values about 7°C lower, (b) daytime (peak) values up to 25°C lower, (c) variable peak-value times (1500 LST for smallest versus 1 h later for three largest), again due to volume to the surface area effect discussed above, and (d) larger midday differences.

Hot-spot day (for both T_o and T_h) results (Fig. 18 a, b) are similar to average-day results, except that diurnal variations are increased (as peak values are higher. Minimum values are only slightly changed) and the expected "erratic" T_h values again arise during the specified over-load hours. The first change is expected, as peak-loads occur during summer daytime hours, while nighttime loads are generally unchanged (from their low values) throughout the year.

Average-day fractional internal heat-generation rates $\dot{Q}_A$ for all DT sizes are virtually identical (Fig. 19a), with peaks at 1400 LST (time of SFO input peak-load). This parameter depends on L and DT resistance, where resistance depends on winding temperature T_w. As fractional changes of L overwhelm those for T_w, the diurnal variation of $\dot{Q}_A$ is thus independent of DT kVA rating/size.

Average-day fractional heat-loss rate to the environment $\dot{Q}_o$, however, is dependent on DT size (Fig. 19b), with smaller daily variations (via reduced day-time maximum and increased nighttime minimum values) for the larger DTs. As weather-factors impact DT surfaces (and not its volume), its effects are again fractionally greater for small DTs, as discussed above. The near-zero $\dot{Q}_o$ value for the smallest DT at 0900 LST arises from the low early morning SFO wind speed (Fig. 5a) that produces a convective loss that just exceeds the then weak solar heating. The heat loss then increases during the warming period, before it decreases during the cooling period (1800 to 0900 LST). Peak heat-losses lag max SFO wind speeds (which peak at 1600 LST, Fig. 5a) due to the high DT thermal inertia, which causes $\dot{Q}_o$ to lag L.

Non-normalized average-day internal heat-generation rate $\dot{q}_A$ (in W), however, is a strong function of kVA rating/size (Fig 20a), especially

during daytime hours, when larger DTs have bigger $\dot{q}_A$ values (as expected). Ratios of daytime max to nighttime min $\dot{q}_A$ values for all four DT sizes are about a factor of three.

All corresponding external heat-loss rate $\dot{q}_o$ values (Fig. 20b) also show higher kVA DTs with larger $\dot{q}_o$ values, as expected. Values dip around 0900 LST due to the growth in solar-heat gain, but then increase during afternoon hours due to the dominance of turbulent heat loss. The time of peak heat loss (1800 LST) is independent of DT size, and lags both the SFO solar heating and wind speed peaks.

Maximum normalized "hot-spot" day $\dot{Q}_A$ and $\dot{Q}_o$ values (Fig. 21 a, b) are similar to average-day results, except for their expected afternoon over-load peaks and generally doubled magnitudes. The unexpected small negative Q_o (heat gain) around 0800 LST for the smallest DT (with its low internal heat generation) results as its turbulent heat loss is less (as SFO speeds are then zero) than its concurrent large early-morning "hot-spot day" solar heating. The non-normalized "hot-spot" day $\dot{q}_A$ and $\dot{q}_o$ results (Fig. 22 a, b) are also similar to average-day results (Fig. 20), except for its expected: (a) "erratic" $\dot{q}_A$ values (again from the specified over-load) and (b) doubled magnitudes.

2) Cooling mode

Four DT-radiator cooling-modes (OA, FA, DFOA, and NDFOA) for a 250 kVA DT in SFO were considered. Results showed (as expected) that T_h values were high during the day and low at night (Fig. 23a). The direct forced oil and air (DFOA) mode shows significantly lower values, as pumps and fans mechanically increase hot-oil mixing towards outer DT surfaces, thus increasing turbulent heat-loss to the air, as seen in Eq. (10). Heat transfer from windings to oil Q_W^- is particularly effective via Eq. (6) as oil is forced into the windings, thus decreasing T_h via Eq. (13). Resulting differences with respect to the other cooling-modes are thus maximum (about 8°C) during noontime hours and minimum during nighttime hours.

The OA and FA modes show similar T_h values (with OA values slightly greater than FA values) through out the diurnal cycle. While their oil flows are the same, OA airflow oil cooling is not aided by fans as is done in the FA mode. Nighttime NDFOA cooling-mode temperatures are similar to the other forced-oil cooling mode (DFOA), but its daytime values are higher. They are also higher than OA and FA values from sunrise to 1700 LST, but are lower at night.

This difference from the OA and FA patterns is due to the NDFOA top-oil that bypasses the hot windings, thus allowing rapid DT-core warming during its peak daytime load period. Its forced oil-flow cooling (compared to natural OA and FA oil-flow cooling) can ultimately transfer more core heat after several hours, and thus it cools more rapidly in the late afternoon than do the other three modes.

Cooling-mode dependence of average-day average-oil temperature T_o, one of the most important temperature for DT energy-efficiency calculations, is determined by input heat-transfer exponents. As indicated in Eq. (33), larger exponents produce lower heat transfers. As the OA cooling mode has the lowest exponent in Table 3, it has the maximum T_o values in Fig. 23b, while the DFOA mode has the lowest T_o values because it has the largest exponent. Unlike the above T_h values (Fig. 23a), all T_o curves are parallel and show expected daytime maximum and nighttime minimum values.

Hot-spot day T_h and T_0 (Fig. 24) values are similar to average-day values, except that both are larger and that a sharp peak exists for T_h at the overload hour (1400 LST). In addition, peak load T_h values are the same for all cooling modes except DFOA, whose slightly higher value is due to a design-feature that results in both rapid cooling (when $L < 1.0$) and warming (during over-load conditions). Both average-day (Fig. 25)

and hot-spot day (Fig. 26) fractional $\dot{q}_A$ and $\dot{q}_O$ values show almost no dependence on DT cooling mode, while their non-fractional values (not shown) would show the dependence seen in the T_h values of Fig. 23a.

3) Climate

DT operations are effected by weather parameters, such as ambient air temperatures, solar radiation, and wind. In addition, weather impacts building type and electrical load, and thus affects both DT load-produced heat-generation and internal DT heat dynamics. Three representative US sites (San Francisco, Boston, and Phoenix) were thus considered for analysis by use of the LBNL03wx model for a 250 kVA DT in FA cooling mode.

Average-day DT coil T_h and oil T_o temperature diurnal variations were generally similar for all three sites (Fig. 27 a, b). Both parameters were always maximum at PHX (in a southwest sunny hot climate that requires large air-conditioning driven input-loads) and lowest at BOS (in a northeast cold climate that requires the smallest input electrical loads). Minimum interior T_h and exterior T_o values at all site occur around 0600 and 0700 LST, respectively (as expected).

While maxima T_h values occur at 1500 at SFO or 1600 LST at PHX and BOS, maxima T_o values are each delayed by 1 h (as again expected).

The earlier SFO T_h-peak arises from its 1 h earlier (compared to PHX and BOS) peak-load. The overlap of BOS and SFO internal T_h values at 0700-0800 LST (Fig. 27a) coincides with a similar overlap in fractional (and hence actual, as kVA values are the same) load (Fig. 7a).

Summer hot-spot day (different for each site) T_h and T_o values also show similar patterns (Fig. 28 a, b) to the average-day values, except that both are much warmer (as expected). In addition, SFO (and not BOS) has the lowest values, due to the onshore flow over the cold California coastal ocean current that produces the lowest hot-spot day ambient air temperatures at SFO (Fig. 7a). PHX and BOS T_h values are 45^{0}C above their corresponding average-day values, while the SFO difference is 10^{0}C smaller; all occur at the time of the peak load. Corresponding T_o differences are 25^{0}C for PHX and BOS and 13^{0}C for SFO.

In addition, the interior hot-day T_h values show: (a) expected isolated 1 h peak values, each of which coincides with its peak load (Fig. 7b), (b) a morning PHX and BOS overlap (as BOS values increase), and (c) an evening BOS and SFO overlap (as BOS values decrease). Both overlaps coincide with overlaps in L values from a large early morning BOS rise and its large afternoon fall. These effects counteract the cooling effect of the lower BOS ambient temperatures.

Average-day fractional heat generation rate (add dot) $\dot{Q}_A$ (Fig. 29a) follows the average-day load pattern (Fig. 7a), but as load losses P are roughly $\propto L^2$, small L differences are amplified. Peak values occur at 1400 LST for SFO and at an hour later for BOS and PHX, consistent with peak L times.

Average DT fractional surface rate of heat losses $\dot{Q}_o$ to the environment (Fig. 29b) show: (a) generally similar patterns for all sites, (b) low values near noon due to DT solar radiation gains, and (c) peak values during late afternoon hours, as high DT thermal inertia retards the loss of stored daytime solar energy (as in urban areas). SFO has the largest early-evening heat loss (at 1800 LST) corresponding to large convective heat losses from its evening sea breeze. The latter PHX maximum heat loss arises from its large nighttime L (due to continued air conditioning usage), which produces a large internal QA (add dot) that must be balanced by a correspondingly large $\dot{Q}_o$.

Hot-spot day $\dot{Q}_A$ and $\dot{Q}_o$ results (Fig. 30 a, b) are similar to average-day results, except that: (a) the assumed L_{max} conditions produces isolated peak $\dot{Q}_A$ values, (b) values are almost doubled (as expected), (c) SFO and BOS have higher late-afternoon peak $\dot{Q}_o$ values than PHX (due to their increased sea breeze wind speeds, Fig. 5b), and (d) different post-

midnight nocturnal $\dot{Q}_0$ values SFO and BOS (due to previous daytime inputs). Peak $\dot{Q}_A$ values occur at 1000, 1400, and 1600 LST for BOS, SFO, and PHX, respectively, in correspondence to peak L values.

Peak-hour T_o and T_h average and hot-spot day results for each LBNL03 model (ts, tw, and wx), site, and kVA value (but not 28 000 kVA) aare shown as deviations (LBNL03 minus IEEE95) in Table 6. Results not previously discussed consist of those for BOS and PHX for DTs other than 250 kVA. In general, weather impacts for peak-hour temperatures are similar to those from the SFO kVA parametric study as: (a) impacts decrease with increasing kVA (due to the higher surface area to volume ratios for small DTs), (2) solar effects increase values, with max impacts in sunny PHX, (c) wind effects decrease values, with max impacts in BOS (has strongest peak-load hour winds), and (d) wind dominates solar (except in sunny PHX), with max net effects in BOS. Net differences are not simply the difference between the two individual effects, due to nonlinear interactions inherent in factor analysis techniques (Alpert and Stein 1992).

4) Aging factor

Weather impacts on DT equivalent annual aging-time E_A for each LBNL03 model, site, and kVA value are shown in Table 7a. All DT aging

times are small (i.e., slow DT deterioration) compared to the above mentioned annual design value of 6000 h, indicating that DT loads are generally low. Weather-induced impacts show PHX with the largest impacts (up to 1713 h). Solar-induced calm-wind deteriorations are: (a) increased over temperature-only values, (b) larger than wind-only times, and (c) decreased with DT size. Windy-condition (without solar-heating) results show: (a) E_A values less than temperature-only times and (b) impacts (deviations from IEEE95 values) that decrease with increasing DT size. With both wind and solar effects, the former dominates. The above values were used to calculate percent-changes from corresponding IEEE95 impacts, and results (Table 7b) show how much solar impacts dominate wind effects.

5. Conclusion

The objective of this research was estimation of electrical DT heat losses with and without consideration of weather effects. The IEEE95 model was thus first translated from BASIC to FORTRAN, producing the new LBNL03 model. Simulated DT temperatures from the new model for a 28 000 kVA DT validation test case were identical to those from the published IEEE95 study. Turbulent DT heat losses due to wind effects and heat gains due to solar radiation effects were then incorporated into LBNL03 to produce the final LBNL03wx model.

A series of yearlong parametric simulations were carried out with LBNL03wx to investigate weather impacts on DT heat energy losses for five DT kVA ratings/sizes, four DT cooling modes, and a representative city in each of three different US climatic regions. Input data included yearlong hourly weather data and corresponding electrical DT electrical loads from previous LBNL simulations. Eight model output DT temperature components and 13 heat fluxes rates were calculated, but the analysis focused on two important (winding hot-spot and average oil) temperatures and heat fluxes (total internal heat generation and DT surface loss to the surrounding environment).

Important results included:

- The new FORTRAN version is exact.
- Interior electrical-load impacts on DT internal heat fluxes and temperatures are more significant than on corresponding outer-skin parameters.
- High DT thermal inertial produces lags between times of (maximum and minimum) interior DT load values and their corresponding impacts on DT temperatures and fluxes. Such lags are close to zero for interior DT parameters, but large for corresponding outer-skin parameters.
- Internal-load variations are stronger than external weather variations, and thus internal and interior DT temperatures and fluxes have larger diurnal variations than do corresponding exterior parameters.
- Solar energy absorption produces increased DT temperatures and fluxes, with maximum effects during daytime hours and with low wind speeds.
- Convective cooling effects on DT temperatures and fluxes are maximum with high daytime wind speeds. During nighttime hours,

however, they dominate solar radiation effects, which exist only as small residuals from the previous daytime solar heating.

- San Francisco convective cooling peaks in late afternoon in conjunction with its late afternoon sea-breeze wind peak.

- Weather impacts on DT internal heat fluxes and temperatures are less significant than on corresponding outer-skin parameters.

- Windy solar-heating cases produce larger DT convective cooling effects than calm solar-heating cases, as heating produces higher temperatures and thus greater cooling rates.

- High DT thermal inertial produces lags between times of (maximum and minimum) external weather parameters and (maximum and minimum) impacts on DT temperatures and fluxes. Such lags are larger for interior DT parameters than for corresponding outer-skin parameters.

- Hot-spot day interior and outer-skin temperatures and fluxes are larger than corresponding average-day values.

- No significant dependence of interior and outer-skin DT temperatures on DT size exists during peak-load daytime hours due to convective cooling.

- DT internal heat-generation is proportional to DT volume, while heat loss to the environment is only proportional to DT surface area, and thus "volume to area ratio" explains the direct and indirect dependences mentioned below.

- Nocturnal internal and outer-skin average-day and hot-spot day DT temperatures increase with increased DT size.

- Fractional internal average-day and hot-spot day DT heat-generation rates are not dependent on DT size, although actual values increase with increased DT size.

- Fractional internal average-day and hot-spot day DT heat-loss rates to the environment decrease with increased DT size.

- Average-day and hot-spot day actual DT heat-loss rates to the environment increase with DT size.

- Average-day and hot-spot day fractional heat-loss rates to the environment are inversely proportional to DT size.

- Average-day daytime internal DT temperatures are strongly dependent on cooling mode. DFOA mode DTs produce the lowest values, with almost no differences during low-load nighttime hours.

- Average-day and hot-spot day outer-skin DT temperatures are only weakly dependent on cooling mode.

- Hot-spot day internal DT temperatures are not dependent on cooling mode.

- Internal fractional DT internal heat-generation and fractional heat-loss rates to the environment are not dependent on cooling mode.

- Average-day and hot-spot day DT internal and outer-skin temperatures are maximum in hot climates and minimum in cold climates.

- Average-day and hot-spot day DT fractional convective heat losses were low near noon at all sites due to DT solar radiation gains and losses peak during early-evening, as high DT thermal inertia retards the loss of stored heat energy at peak load hours.

- SFO had the largest early-evening heat loss, corresponding to large convective heat losses from its evening sea breeze.

- Aging rates for all DTs are low, as solar-heating effects are compensated by turbulent wind cooling.

- Weather impacts on aging are particularly large for small DTs.

- Increased aging caused by solar heat indicate that painting transformers light colors may be important for small DTs.

Future studies could consider additional DT designs and loads; a wider range of geographic/weather conditions; and micro-climatic effects (not rely solely on NWS sites). Other weather effects to be studied include humidity, cloud, precipitation, and incoming infrared DT absorption.

With the improved LBNL03wx model for calculation of DT temperatures, fluxes, and aging rates, and given the large geographic variability of weather impacts, future applications should aid DOE in development of feasible DT efficiency standards. Various DT model input and output parameters, e.g., aging rates, temperatures, maximum load rates, and energy losses, are also important in DT economic analyses. Future efforts should thus use the new model to determine more cost-effective uses of electrical-distribution transformers.

References

Acker, C. R., 1976: Transformers insulation and transformer life expectancy – A more comprehensive concept. IEEE PES Winter Meeting and Tesla Symposium, New York, NY, 23 pp.

Alpert, P., and U. Stein 1992: Factor separation in numerical simulations. *J. Atmos. Sci.*, **50**, 2107-2115.

ASHRAE, 1985: ASHRAE handbook of fundamentals. Atlanta, GA, 178 pp.

Aubin, J., and T. Langhame, 1992: Effect of oil viscosity on transformer loading capability at low ambient temperature. *IEEE Transactions on Power Delivery*, **7**, 516-524.

Barnes, P. R., S. Das, B. W. McConnel, and J. W. Van Dyke, 1997: Supplement to the "Determination Analysis" (ORNL-6847) and Analysis of the NEMA Efficiency Standard for Distribution Transformers. ORNL-6925, Oak Ridge National Laboratory, Oak Ridge, TN, 128 pp.

Barnes, P. R., J. W. Van Dyke, B. W. McConnel, S. M. Cohon, and S. L. Purucker, 1994: The feasibility of replacing or upgrading utility distribution transformers during routine maintenance. ORNL-6804/R1, Oak Ridge National Laboratory, Oak Ridge, TN, 134 pp.

Barnes, P. R., J. W. Van Dyke, B. W. McConnel, and S. Das, 1996: Determination analysis of energy conservation standards for distribution transformers. ORNL-6847, Oak Ridge National Laboratory, Oak Ridge, TN, 221 pp.

Barnes, P. R., J. W. Van Dyke, B. W. McConnell, S. M. Cohon, and S. L. Purucker, 1995: The Feasibility of replacing or upgrading utility distribution transformers during routine maintenance. Martin Marietta Energy Systems, Oak Ridge National Laboratory, 42 pp.

Beaumont, R., 1988: Losses in transformers and reactors. Unpublished manuscript, 16 pp.

Cooney, W. H., 1925: Predetermination of self-cooled oil-immersed transformers before conditions are constant. *AIEE Transactions*, **44**, 611-18.

Doherty, R. E., and Carter, E. S., 1942: Effects of altitude on temperature rise. *AIEE Transactions*, **43**, 824-839.

DTREA, 2002A: US Department of Energy office of building technology, state, and community program. http://www.eren.doe.gov/buildings/codes_standards/applbrf/pdfs/ea_update.pdf.

Dusinberre, G. M., 1961: Heat transfer calculations by finite differences. Unpublished report, Scranton, PA, 33 pp.

EIA, 2002a: Introduction *Electric Power Industry – 1999.* Energy Information Administration. http://www.eia.doe.gov/cneaf/electricity/epav1/intro.html.

EIA, 2002b: *US Electric utility sales and revenue to ultimate consumers*, 1999. Energy Information Administration. http:// www. eia.doe. gov/cneaf/electricity/epav1/fig16 html.

Feinberg, R., 1979. *Modern Power Transformer Practice*, Wiley, New York, 374 pp.

Frank, J. E., and W. O. Dwyer, 1913: The Temperature rise of stationary induction apparatus as influenced by the effects of temperature, barometric pressure, and humidity of the cooling medium. *AIEE Transactions*, **32**, 235-258.

Ghisalberti, L., and A. Kondjoyan, 1999: Convective heat transfer coefficients between air flow and a short cylinder: Effect of air velocity, turbulence, body shape, dimensions, and position in the flow. *J. Food Engin.* **42**, 33-44.

Holland, S. A., 1992: Calculating stray losses in power transformers using surface impedance with finite elements. *IEEE Transactions on Magnetics.*, **28**, 1355-1358.

Harrison, T. H., 1988: Transformer loss reduction, unpublished paper, 13 pp.

IEEE, 1981: Guide for loading mineral-oil-immersed transformers up to and including 100 MVA with 55°C or 65°C average winding rise. Institute of Electrical and Electronic Engineers, *333 pp.*

IEEE, 1995: Guide for loading mineral-oil-immersed transformers. Institute of Electrical and Electronic Engineers, 235 pp

Joseph, D. H, 1995: The clearness index concept and its place in the HVAC industry. Aust. Refrig., Air Cond., and Heat, **49**, 22-34.

Kreith F., and M. S. Bohn, 1997: *Principles of Heat Transfer.* 5th edition. Boston, MA: PWS Publishing Company, 120 pp.

Marion, W., and K. Urban, 1995: Users manual for TMY2s. National Renewable Energy Laboratory, Golden, CO, 35 pp.

McNutt, W. J., 1992: Insulation thermal life considerations for transformer loading guides. *IEEE Transactions on Power Delivery*, **7**, 392-401.

Montsinger, V. M., 1930: Loading transformers by temperature. *AIEE Transactions*, **49**, 776-792.

Montsinger, V. M., and P. M. Ketchum, 1942: Emergency overloading of air cooled oil-immersed power transformers. *AIEE Transactions*, **61**, 906-916.

Morgan, V. T., 1975: The overall convective heat transfer from smooth circular cylinders. *Adv. Heat Transfer*, **8**, 199-264.

Narbutovskih, P., 1947: Simplified graphical method of computing thermal Transients. *AEEE Transactions*, **66**, 78-83.

NEMA, 1996: Guide for determining energy efficiency for distribution transformers, NEMA standards publication TP 1-1996, National Electrical Manufacturers Association, Rosslyn, VA, 129 pp.

Pierce, L. W., 1992: An investigation of the thermal performance of an oil filled transformer winding. *IEEE Transactions on Power Delivery*, **7**, 1347-1358.

Pierce, L. W., 1994: Predicting liquid filled transformer loading capability, *IEEE Transactions on Industry Applications*, **30**, 170-178.

Quarmby, A., and A. Al-Fakhri, 1980: Effects of finite length on forced convection heat transfer from cylinders. *Inter. J. of Heat and Mass Transfer*, **23**, 463-469.

Skinner, C. E., and L. Chubb, 1913: Effect of air temperature, barometric pressure, and humidity on the temperature rise of electric apparatus. *AIEE Transactions*, **32**, 279-288.

Vogel, F.J., and P. Narbutvskih, 1942: Hot-spot winding temperature in self-cooled oil-insulated transformers. *AIEE Transactions*, **61**, 133-136.

Zukauskas, A. A., 1972: Heat transfer from tubes in cross flow. *Adv. Heat Transfer*, **8**, 116-133.

Appendix A. List of Symbols

A	Transformer surface area [m^2]
A_d	Cylindrical transformer top and side surface area [m^2]
A_E	Equivalent aging acceleration factor [dimensionless]
A_g	Aging acceleration factor [dimensionless]
B	Constant in viscosity calculation [dimensionless]
C	Transformer heat capacity [$J\ K^{-1}$]
C_h	Convection heat transfer coefficient [$W\ m^{-2}\ K^{-1}$]
c	Specific heat [$J\ kg^{-1}\ K^{-1}$]
D	Cylindrical transformer diameter [m]
E	Fractional I^2R losses [dimensionless]
E_A	Equivalent aging time [dimensionless]
F	Constant for viscosity calculation [dimensionless]
H	Transformer height [m]
h	Winding height to hot spot location [dimensionless]
i	Electric current [A]
L	Fractional hourly load [dimensionless]
L_{max}	Peak fractional hourly load [dimensionless]
m	Mass [kg]
N	Number of day in year [dimensionless]
Nu	Nusselt number [dimensionless]
P	Heat loss at unit load [W]

List of Symbols (continued)

Q_a	Heat absorbed by tank, core, and oil [W s]
Q_d	Diffuse solar transformer heat gain rate [W]
Q_i	Direct solar transformer heat gain rate [W]
Q^+	Heat generation [W s]
Q^-	Heat lost [W s]
Q_u^-	Convective heat lost [W s]
$\dot{Q}$	Normalized (by P_A) heat generation/loss rate [dimensionless]
$\dot{q}$	Heat generation/loss rate [W]
R_d	Diffuse horizontal solar radiation [W m^{-2}]
Re	Reynolds number [dimensionless]
R_i	Direct normal solar radiation [W m^{-2}]
T	Temperature [°C]
T_b	Base temperature for losses [°C]
T_k	Resistance temperature correction: 234.5 °C for Copper and 225.0 °C for aluminum)
T_p	Temperature of oil adjacent to winding hot spot [°C]
t	Time [s]
U	Wind speed [m s^{-1}]
V	Voltage [V]

List of Symbols (continued)

V_O	Oil volume [m^3]
x	Exponent in equation for temperature rise of oil at top of duct over bottom oil temperature [dimensionless]
y	Exponent in equation of total loss versus average oil rise over ambient [dimensionless]
Z	Zenith angle [deg]
z	Exponent in temperature difference of oil from top to bottom of radiator (0.5 for OA and FA; 1.0 for NDFOA and DFOA; dimensionless]
α	Albedo [dimensionless]
γ	Fractional temperature correction for heat losses (dimensionless]
ζ_w	Ratio of temperature difference between windings and fluid in cooling ducts to rated difference [dimensionless].
χ_h	Ratio of temperature difference between maximum of windings and of adjacent oil, to rated difference [dimensionless]
λ	Atmospheric thermal conductivity [W m^{-1} K^{-1}]
μ	Dynamic viscosity coefficient [N s m^{-2}]
ρ	Air density [kg m^{-3}]
ΔT_{Ba}	Bottom oil temperature rise over ambient [°C]
ΔT_{DB}	Winding duct oil temperature rise over bottom oil [°C]
ΔT_{hp}	Winding hottest spot rise over oil at hottest spot location [°C]

List of Symbols (continued)

ΔT_{hT}	Hot-spot winding temperature rise over ambient [°C]
ΔT_{oa}	Average-oil temperature rise over ambient air [°C]
ΔT_{PB}	Oil temperatures rise at winding hottest spot location over
ΔT_{Ta}	Top-oil temperature rise over ambient air temperature [°C]
ΔT_{TB}	Oil temperatures difference from radiator top to bottom [°C]
	bottom oil [°C]
ΔT_{Wa}	Winding temperature rise over ambient air temperature [°C]
Δt	Time increment [s]
τ_W	Winding time constant [s]
ϕ	Latitude angle [degree]
δ	Solar declination angle [degree]
ω	Hour angle [degree]
$( )^n$	Time step
$( )_A$	Total
$( )_a$	Atmosphere
$( )_B$	Bottom oil
$( )_c$	Core
$( )_D$	Duct oil top
$( )_d$	Average cooling duct
$( )_e$	Eddy effect
$( )_h$	Hot spot
$( )_o$	Oil

List of Symbols (continued)

$( )_R$	Radiation
$( )_S$	Stray effects
$( )_T$	Top oil
$( )_t$	Tank
$( )_w$	Winding
$\tilde{( )}$	Rated
$( )_x$	Over-excitation state
$\dot{( )}$	Heat generation/loss rate
$( )'$	Correction term

Appendix B. Acronyms

ANSI	American National Institute of Standards
ASHRAE	American Society of Heating, Refrigeration and Air-Conditioning
BOS	Boston
CBECS	Commercial Building Energy Consumption Survey
DOE	Department of Energy
DT	Distribution transformers
DTREA	Distribution Transformers Rulemaking Engineering Analysis
EIA	Energy Information Administration
IR	Infrared radiation
IREQ	Institute de Recherché d'Hydrio-Quebec
IEEE	Institute of Electrical and Electronics Engineers
kVA	Kilo-volt ampere
LBNL	Lawrence Berkeley National Laboratory
NSRDB	National Solar Radiation Data Base
NEMA	National Electrical Manufacturers Association
PHX	Phoenix
SFO	San Francisco

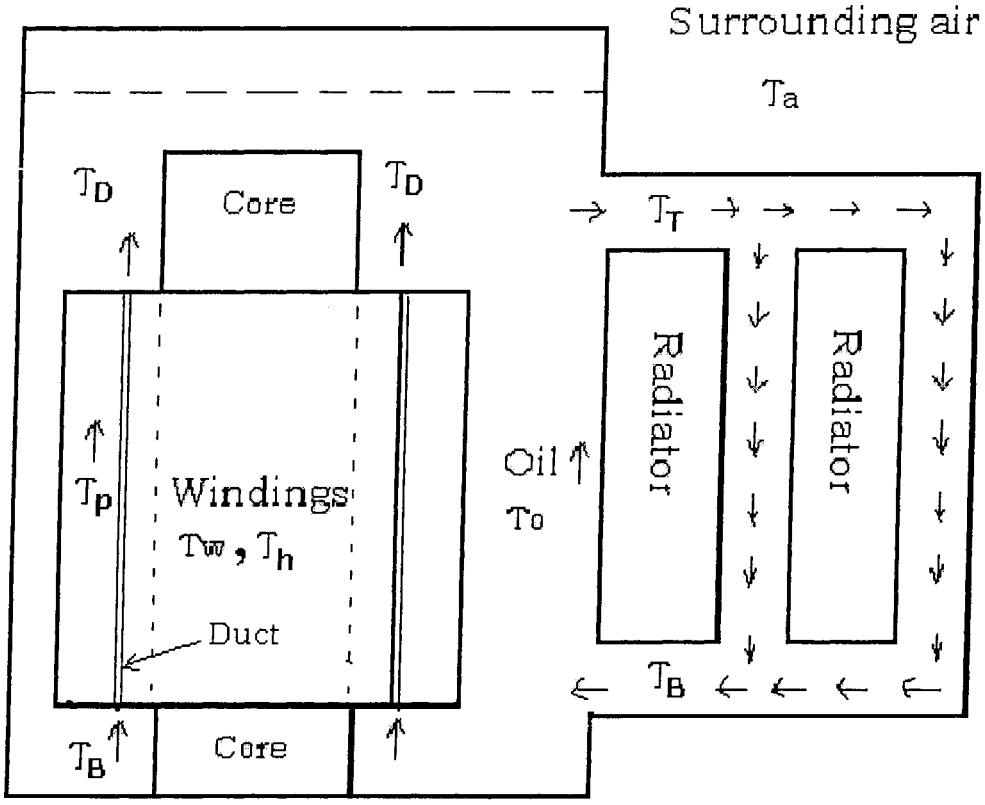

Fig. 1. DT fluid flow (arrows) schematic and temperatures (Ts).

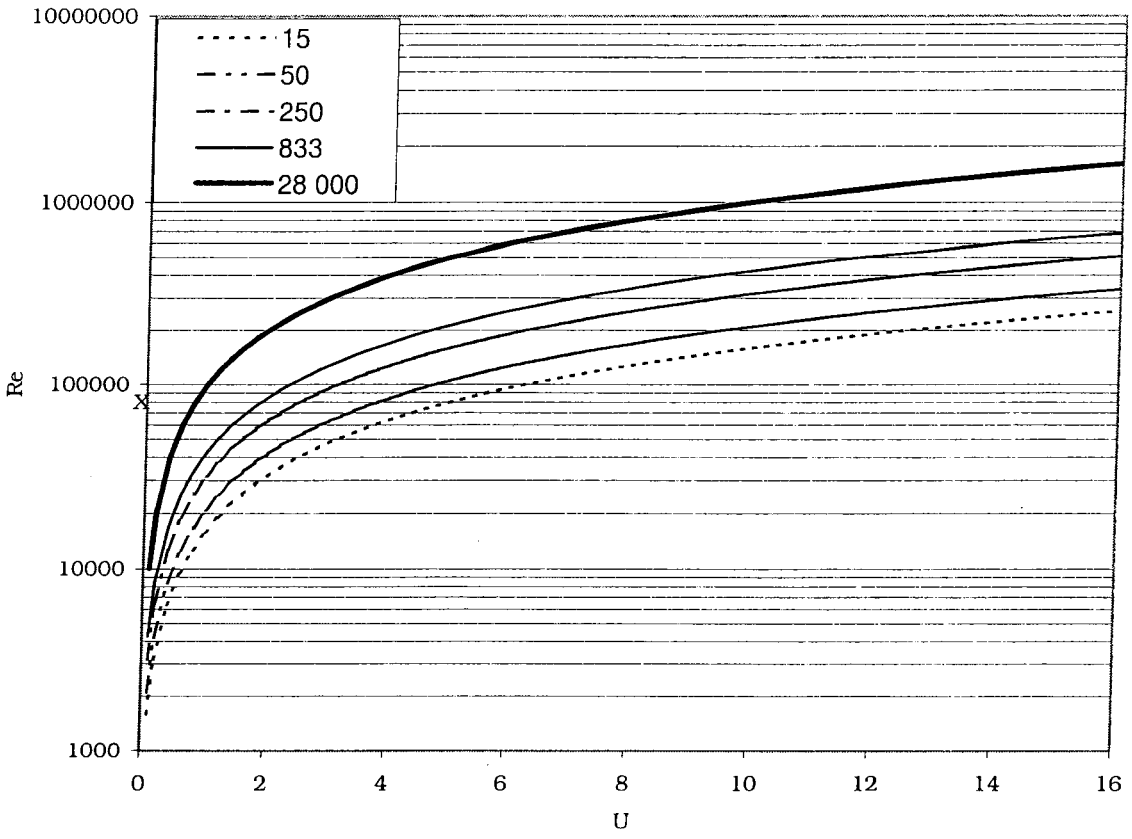

Fig. 2. Reynolds number Re as a function of wind speed U (m s^{-1}) and DT size (kVA) (from Kreith and Bohn 1997), with the limiting Re shown by x.

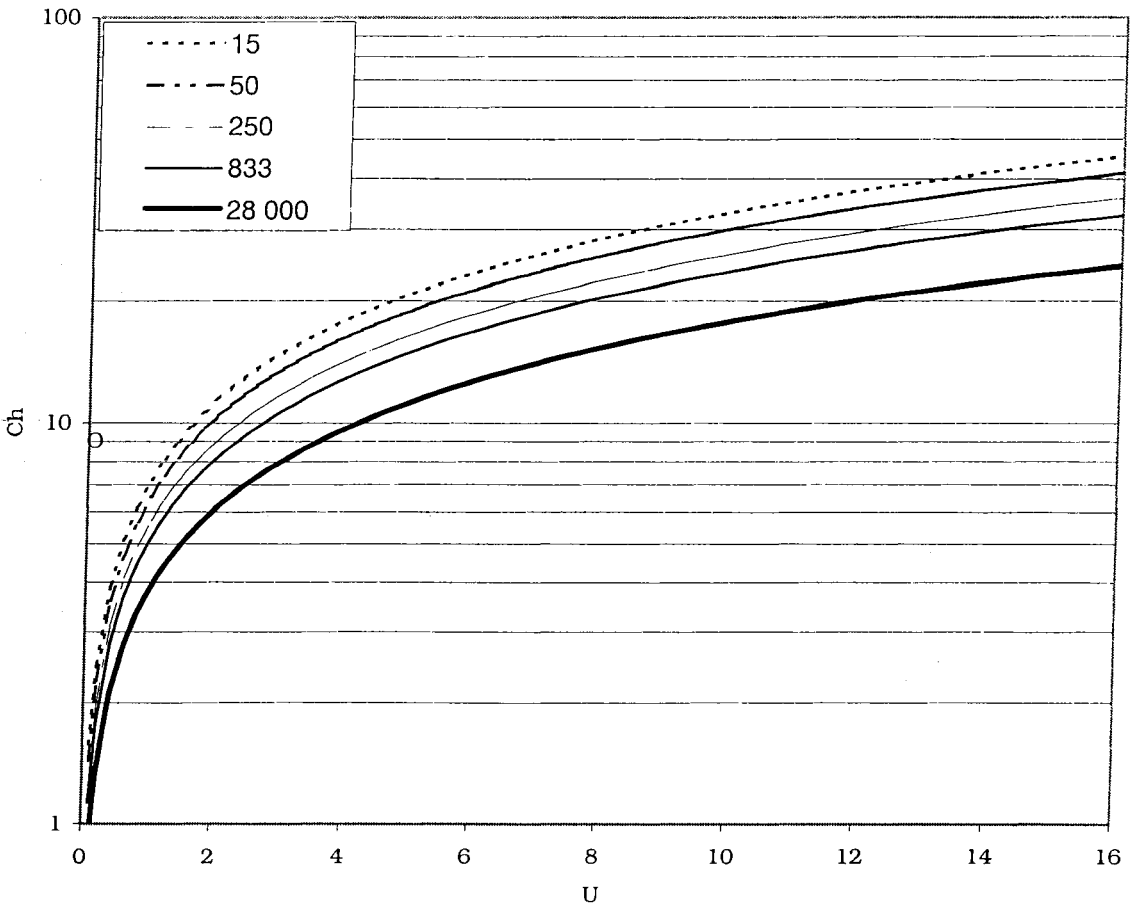

Fig. 3. Convective heat transfer coefficient C_h (W m^{-2} C^{-1}) as function of wind speed U (m s^{-1}) and DT sizes (kVA) (from Zukauskas 1972), where o represents empirical calm-case value of C_o.

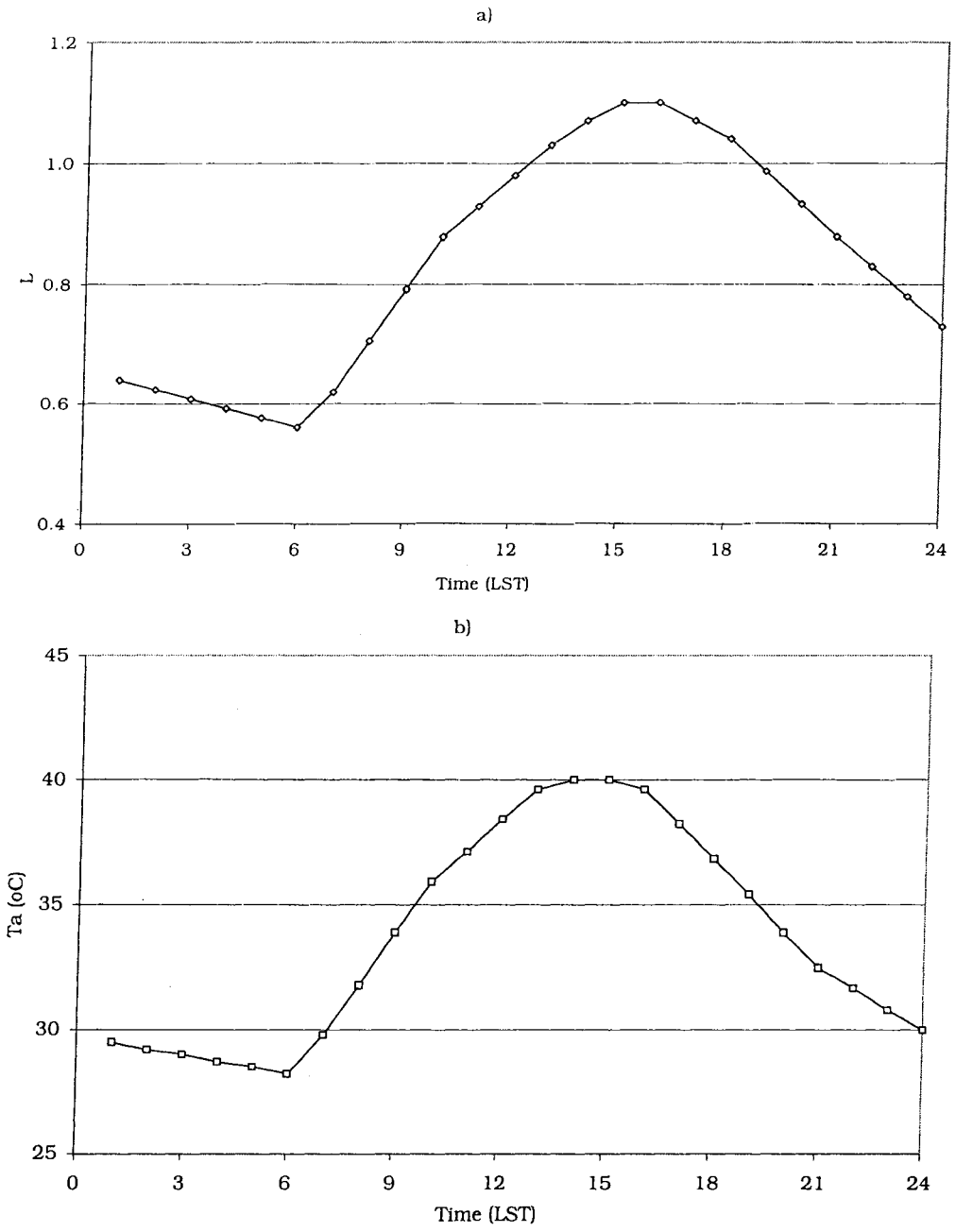

Fig. 4. IEEE95 test-case input values of: (a) fractional electrical load L and (b) ambient temperature T_a.

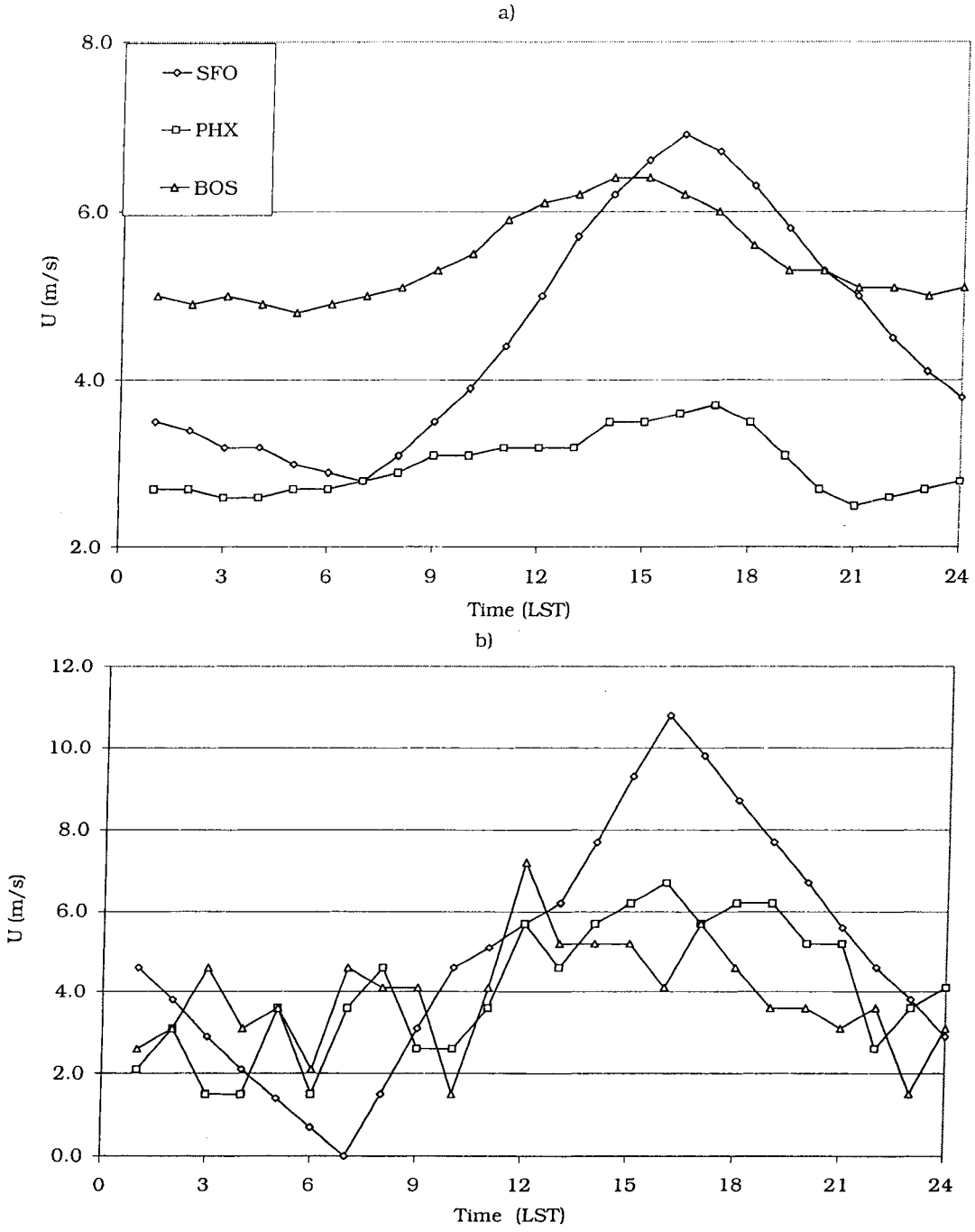

Fig. 5. Wind speed input values for SFO, PHX, and BOS for:

(a) average-day and (b) hot-spot day.

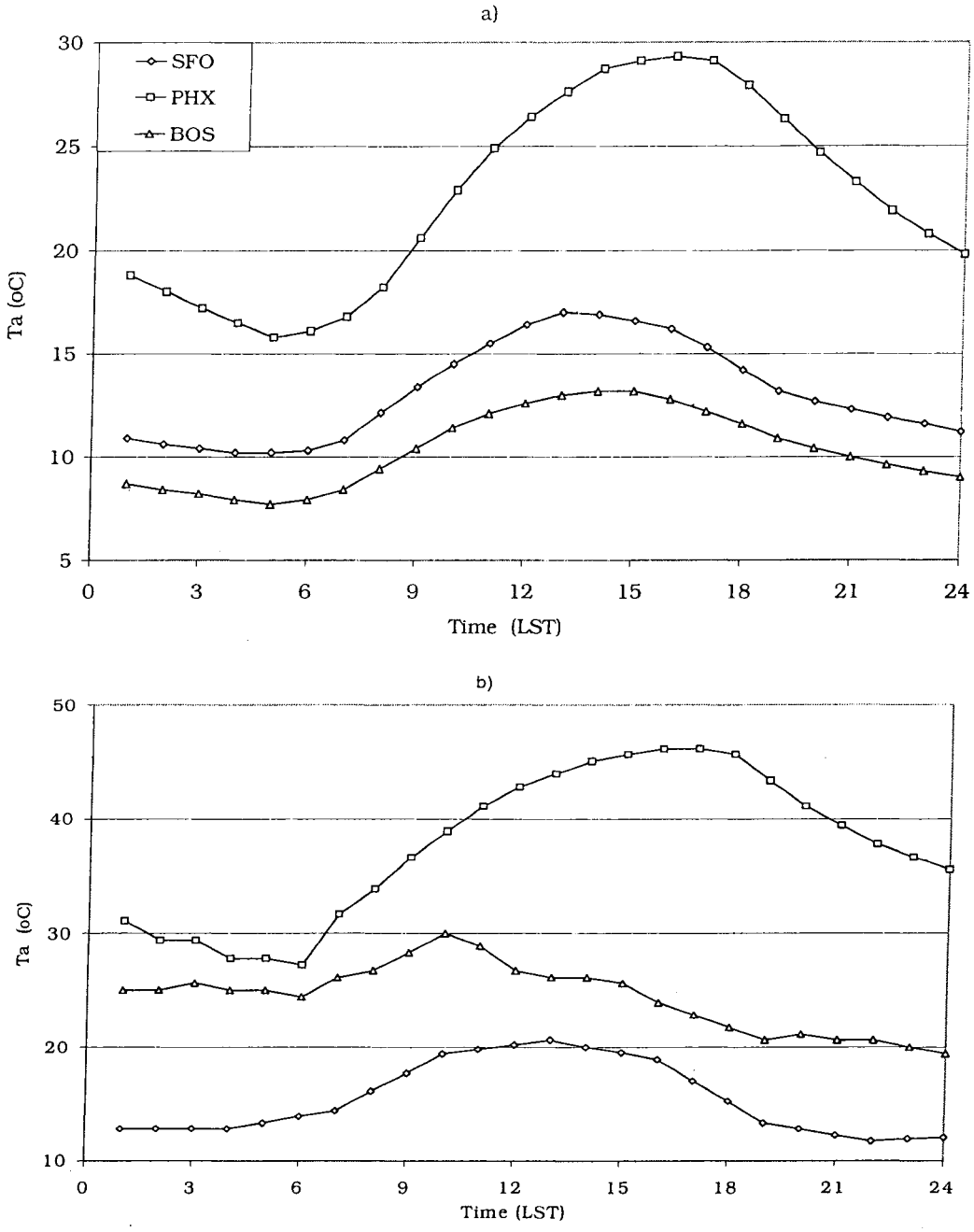

Fig. 6. Ambient temperature input values for SFO, PHX, and BOS for: (a) average-day and (b) hot-spot day.

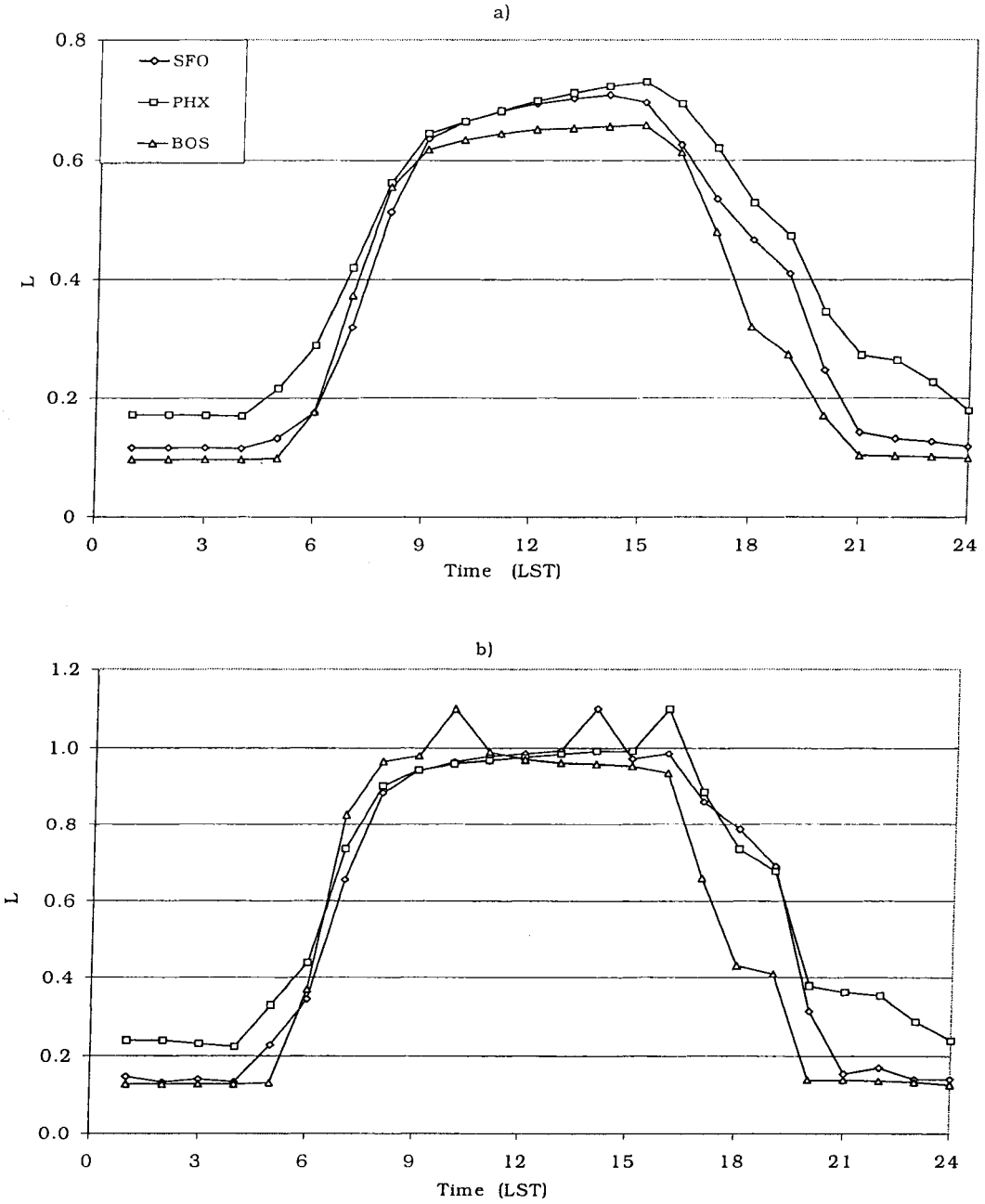

Fig 7. Fractional electrical input load values for SFO, PHX, and BOS for: (a) average-day and (b) hot-spot day.

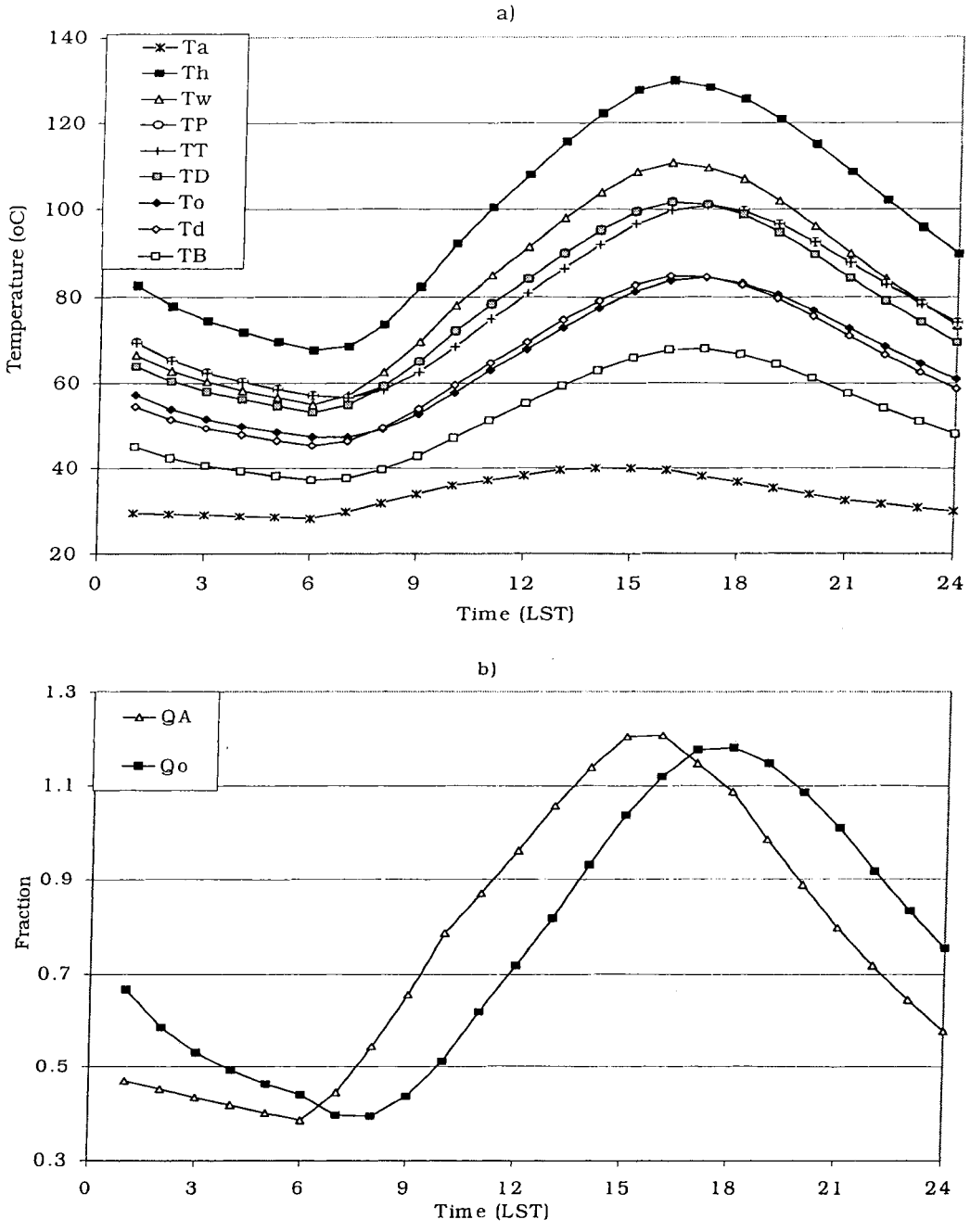

Fig. 8. IEEE95 test case results for a 28 000 kVA DT in FA cooling mode for: (a) temperatures (°C) and (b) heat generation ($\dot{Q}_A$)/ loss ($\dot{Q}_o$) rate.

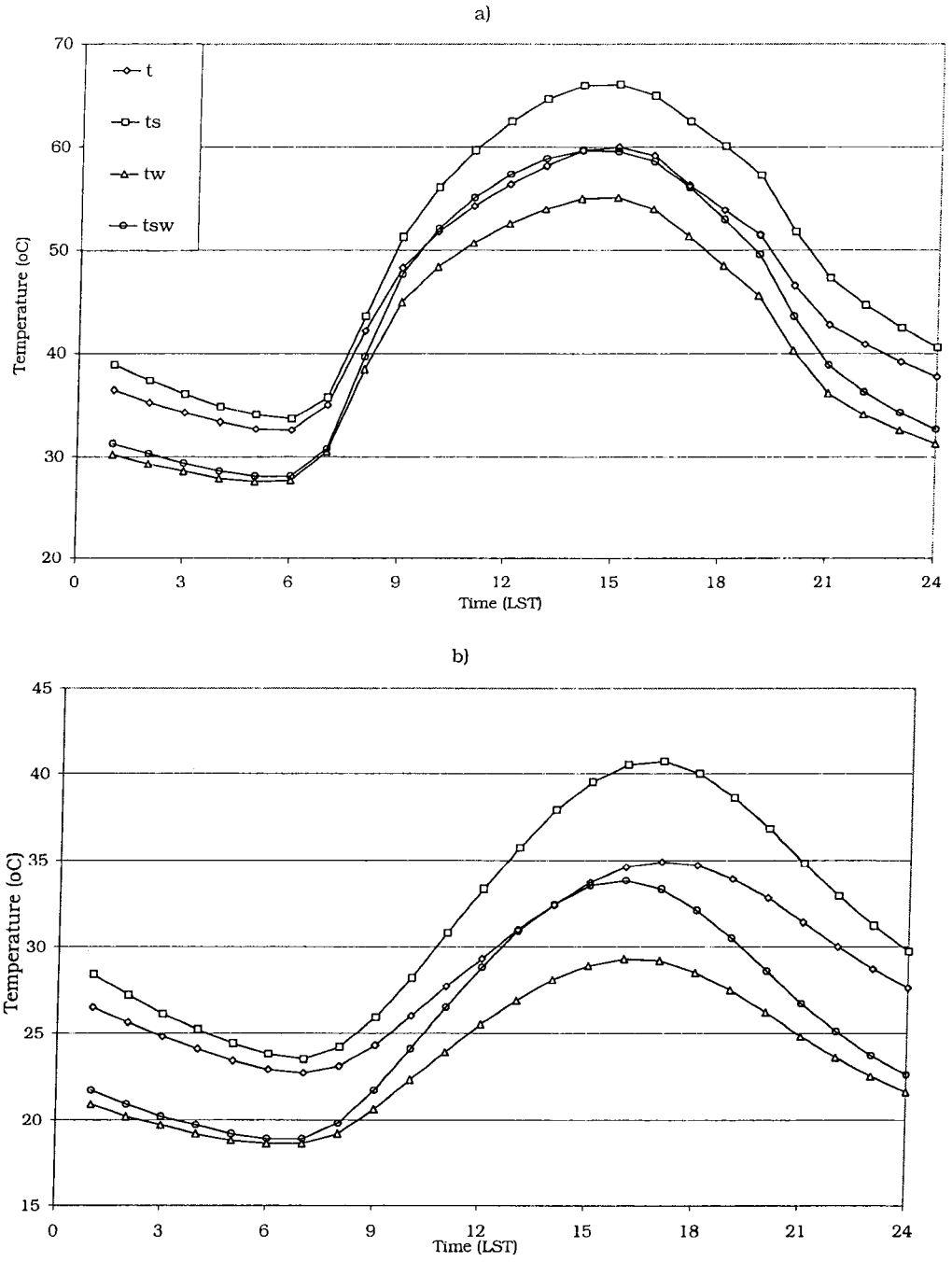

Fig. 9. Average-day temperatures for a 250 kVA DT in FA cooling mode at SFO as a function of weather effect for: (a) T_h and (b) T_o.

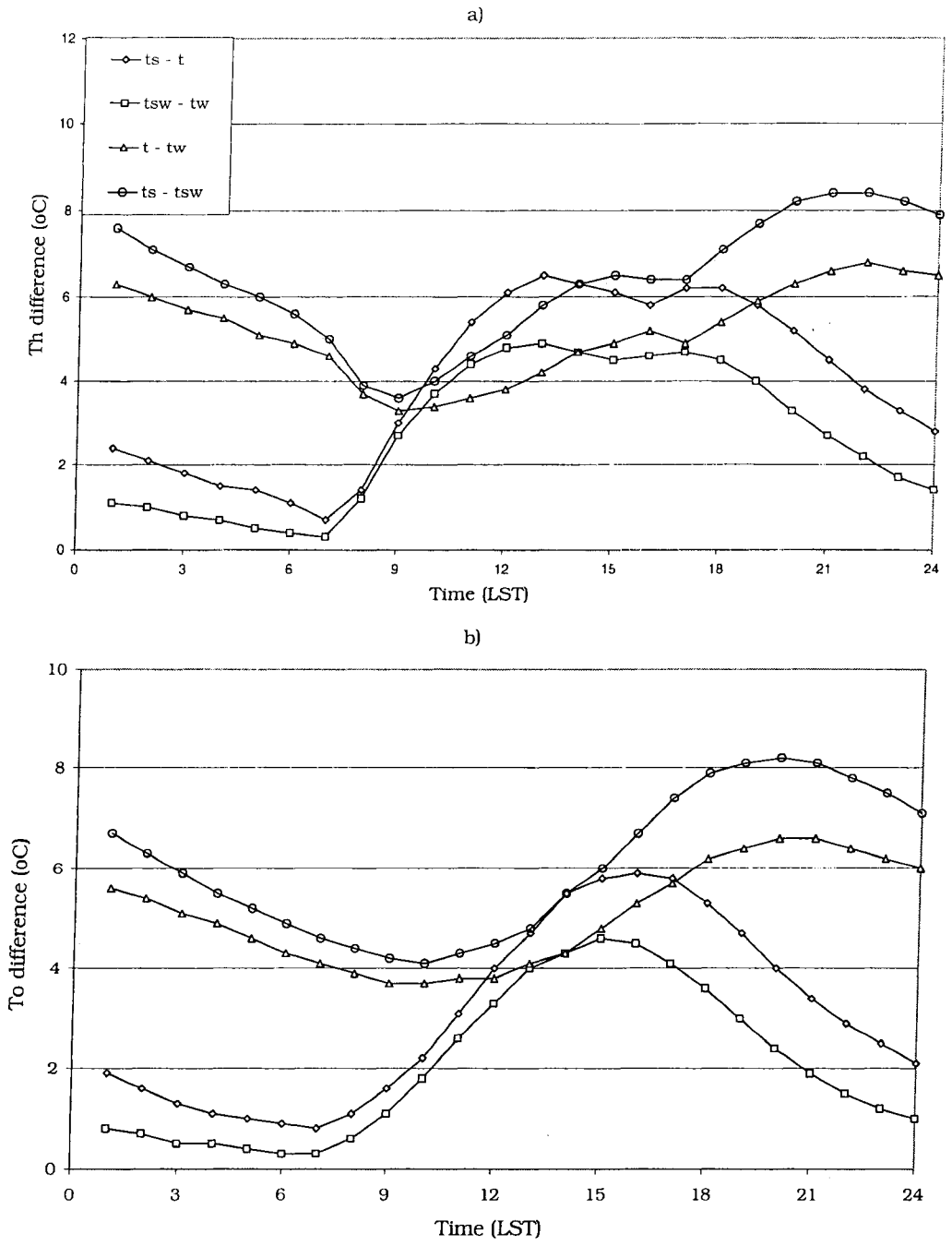

Fig. 10. Average-day temperature differences for a 250 kVA DT in FA cooling mode at SFO as function of weather effect for: a) T_o and b) T_h.

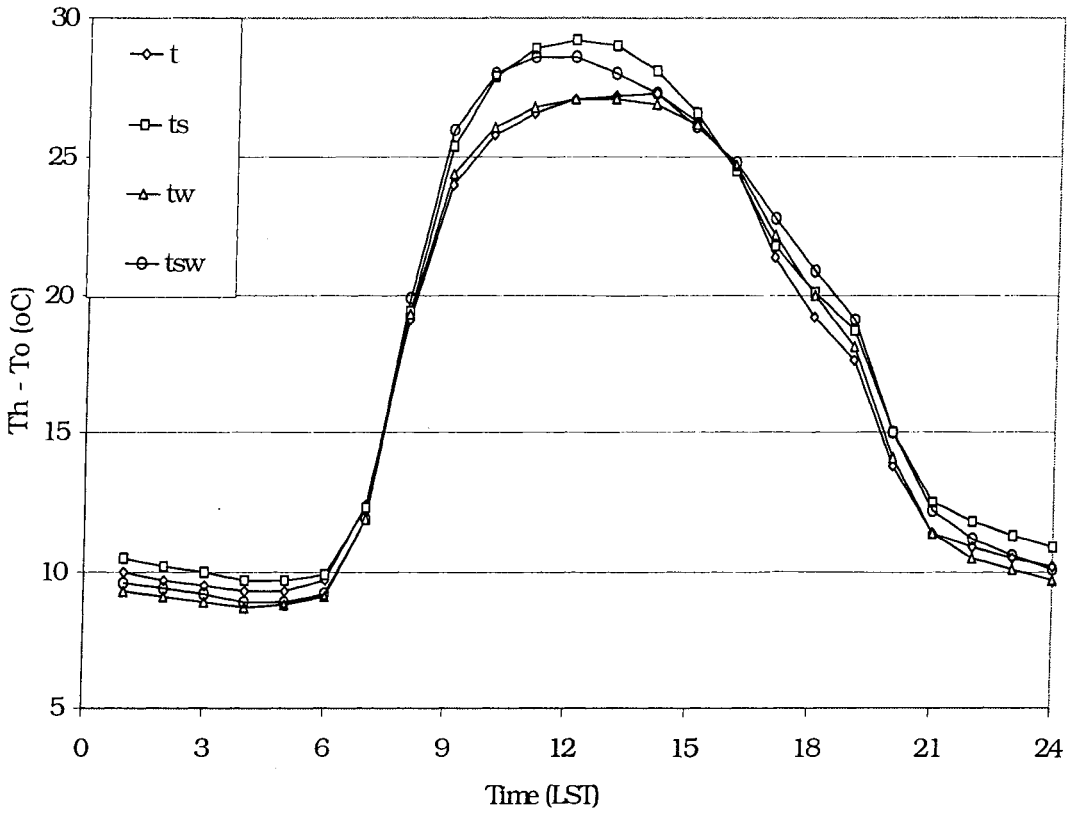

Fig. 11. Average-day temperature difference between T_h and T_o for 250 kVA DT in FA cooling mode at SFO as function of weather effects.

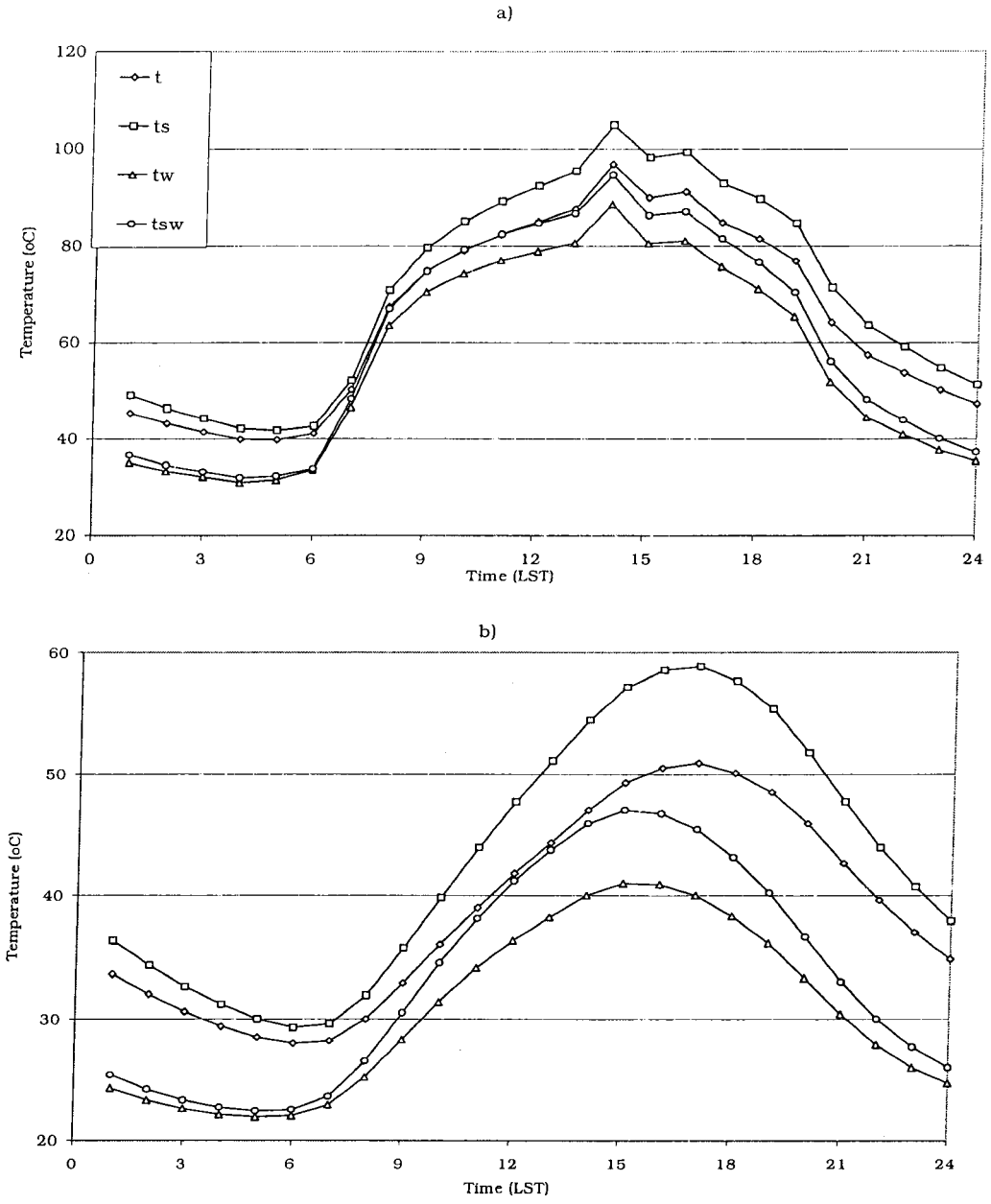

Fig. 12. Hot-spot day DT temperatures for 250 kVA in FA cooling mode at SFO as a function of weather effect for: a) T_o and b) T_h.

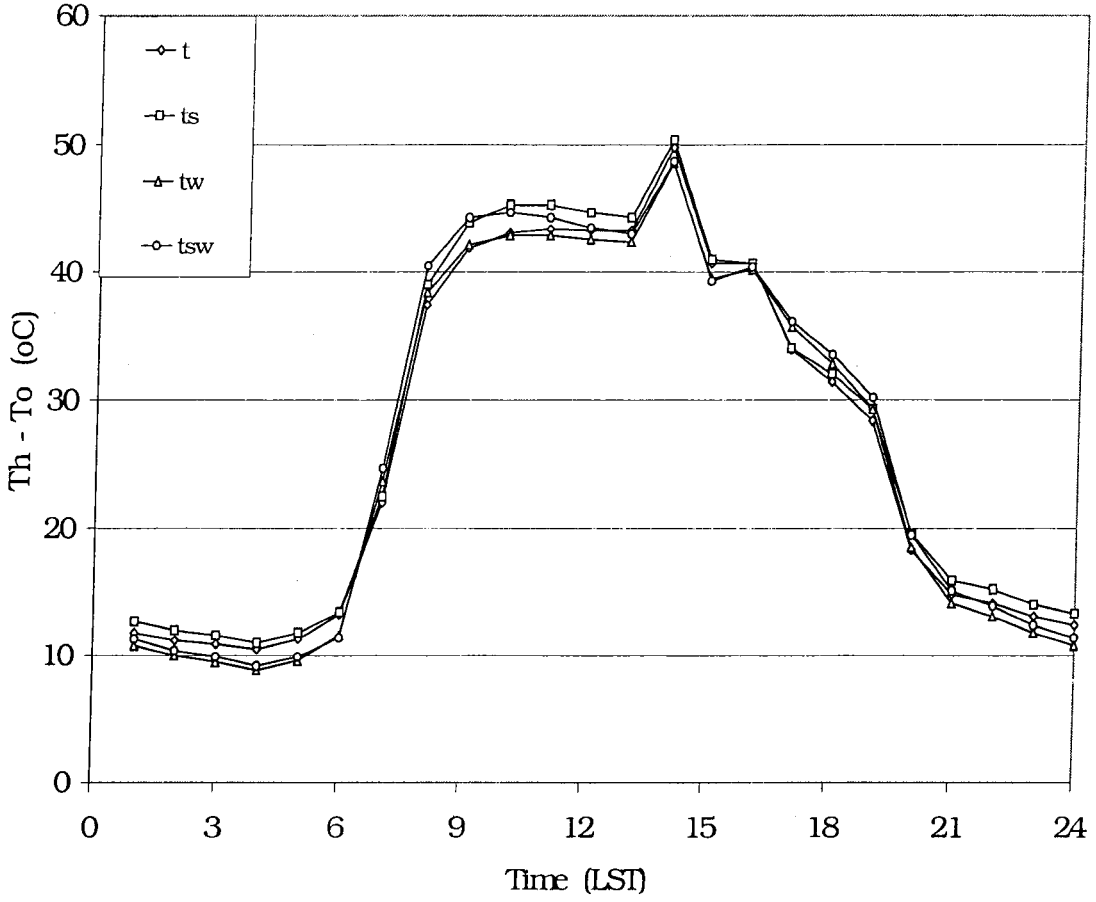

Fig. 13. Hot-spot day Temperature difference between T_h and T_o for 250 kVA DT in FA cooling mode at SFO as function of weather effects.

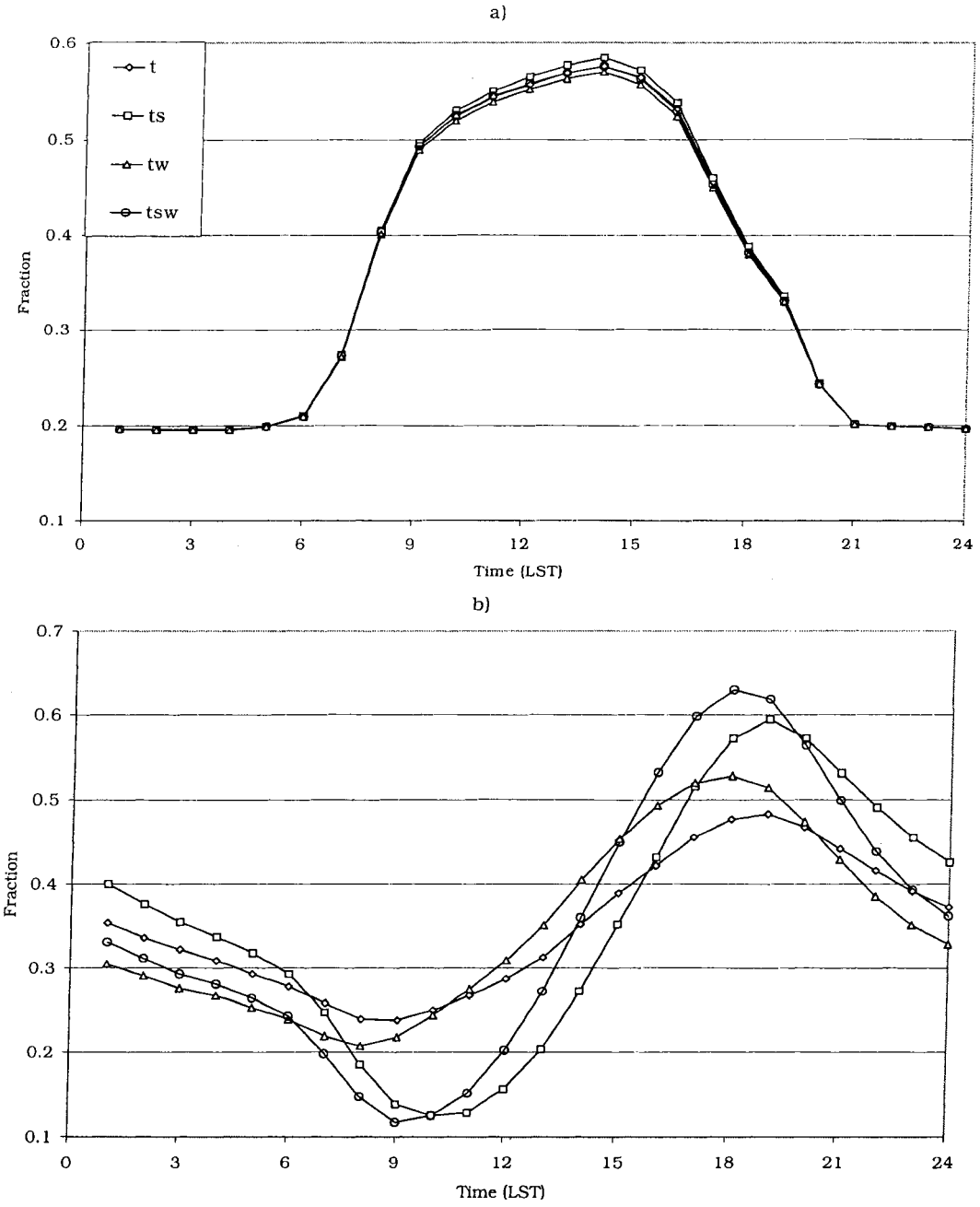

Fig. 14. Average-day heat generation/loss rate for 250 kVA DT in FA cooling mode at SFO as a function of weather effect for: a) $\dot{Q}_A$ and b) $\dot{Q}_O$.

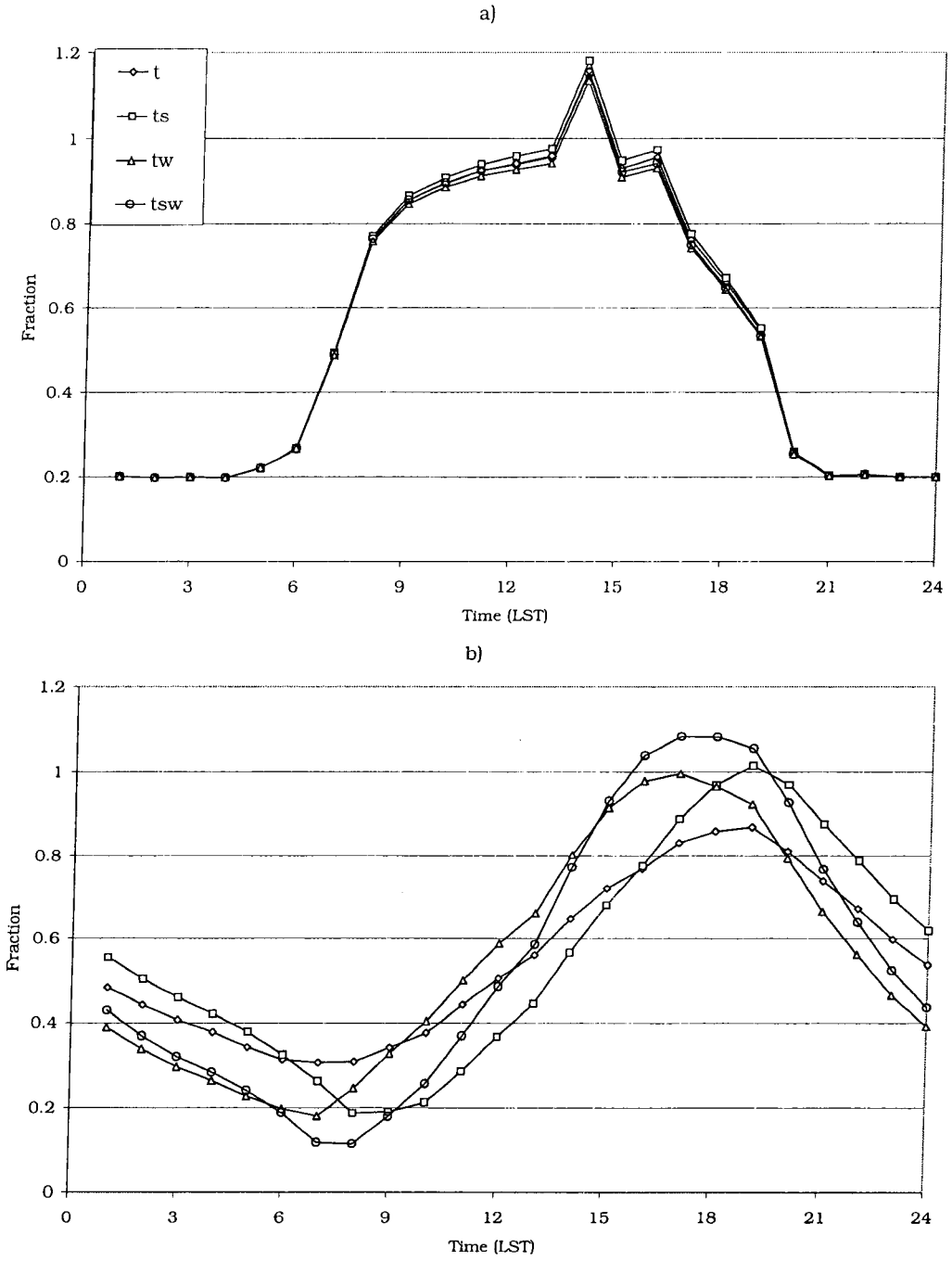

Fig. 15. Hot-spot day heat generation/loss rate for 250 kVA DT in FA cooling mode at SFO as a function of weather effect for: a) $\dot{Q}_A$ and b) $\dot{Q}_o$.

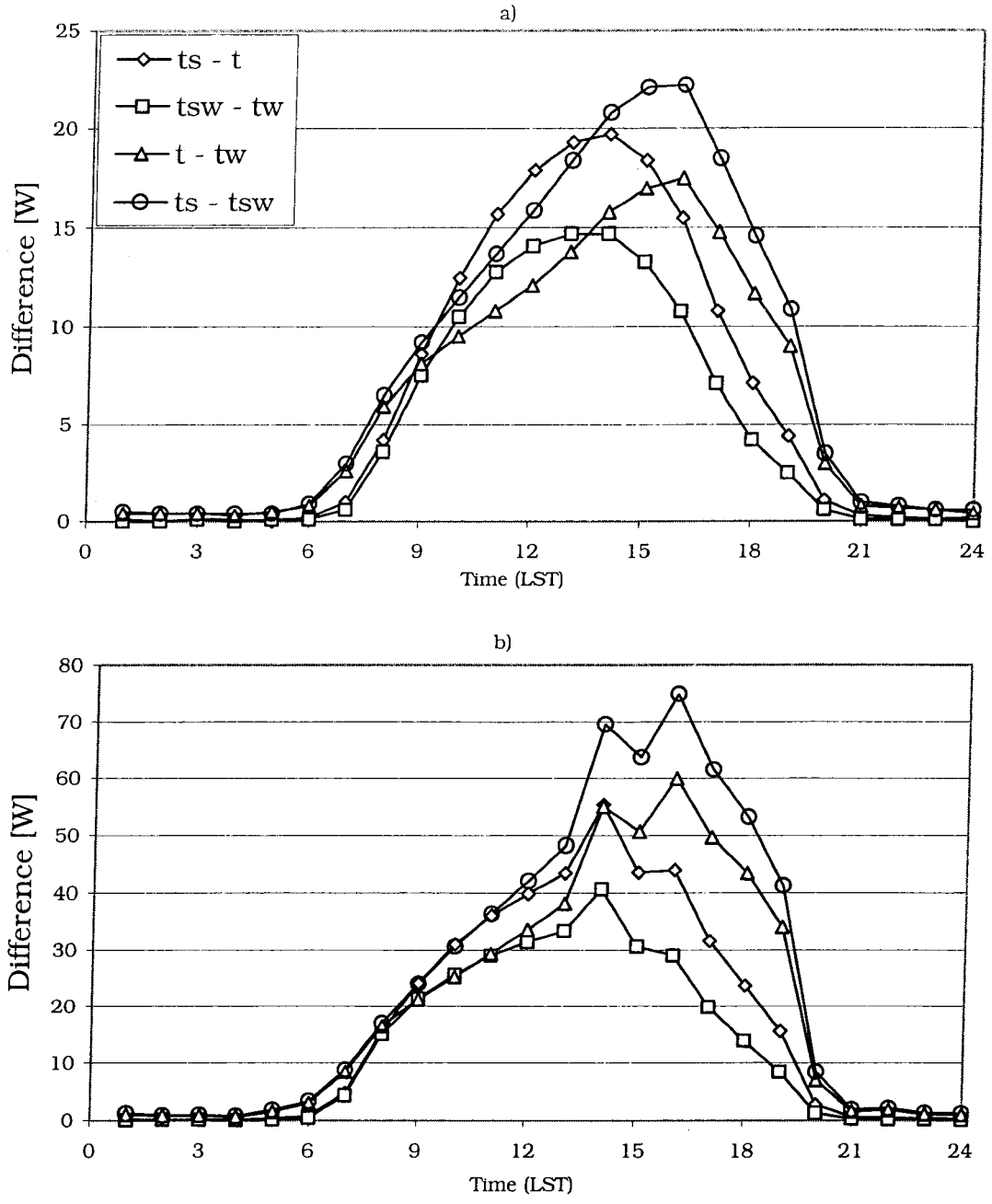

Fig. 16. Heat generation rate ($\dot{q}_A$) difference for 250 kVA DT in FA cooling mode at SFO as function of weather effects for: (a) average-day and (b) hot-spot day.

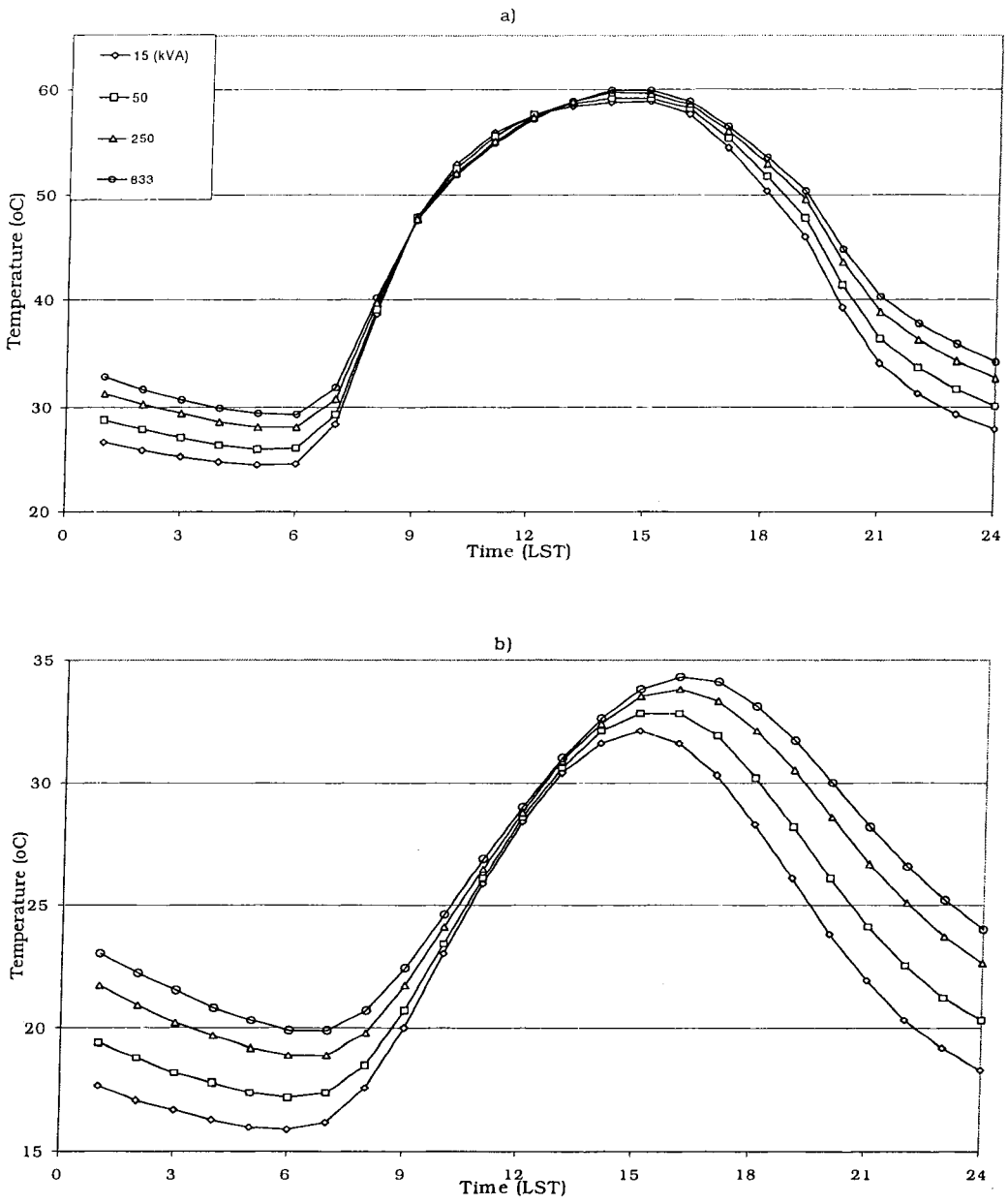

Fig. 17. LBNL03wx average-day temperatures for 15, 50, 250, and 833 kVA DTs in FA cooling mode at SFO for: (a) T_h and (b) T_o.

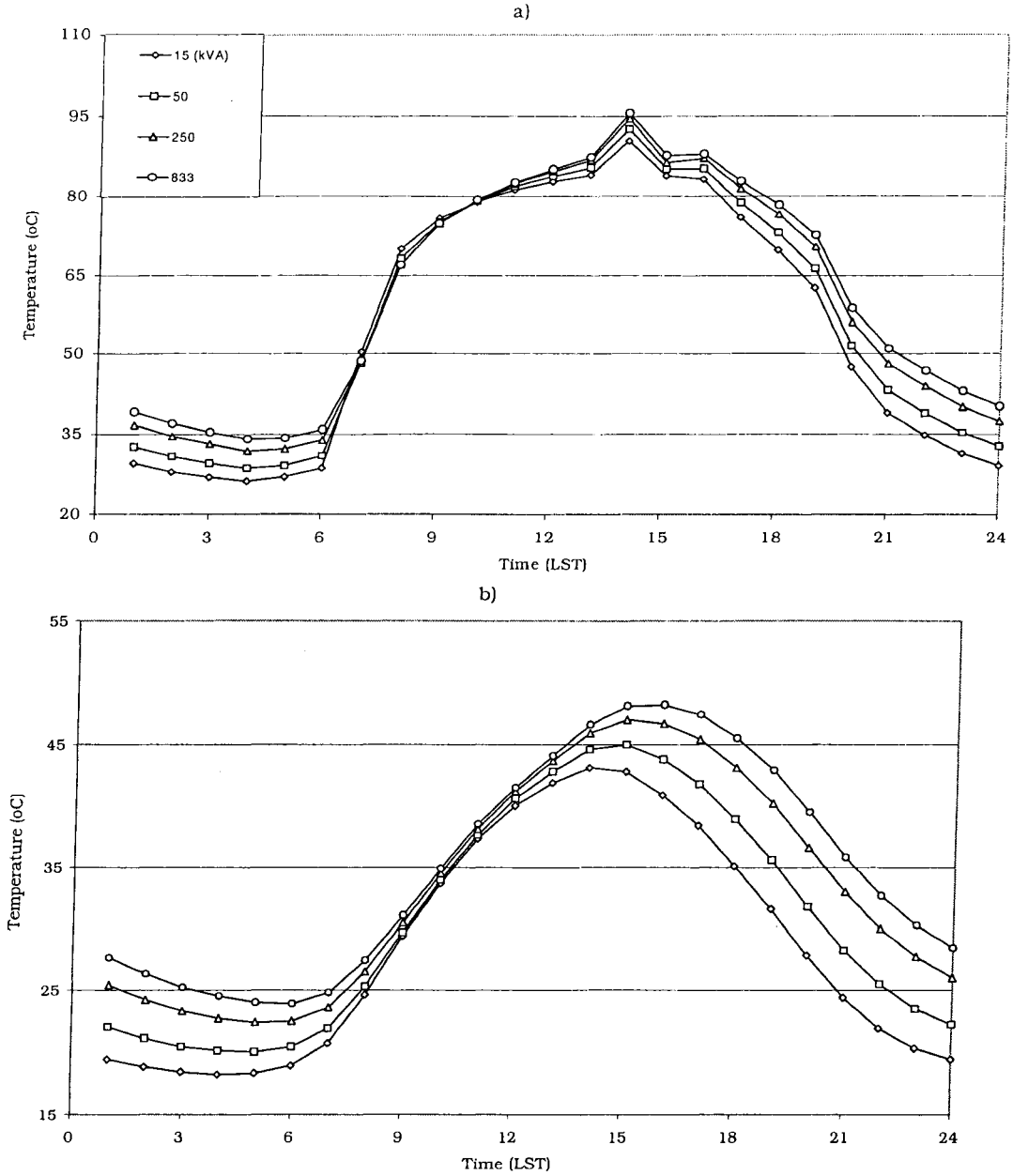

Fig. 18. LBNL03wx hot-spot day temperatures for 15, 50, 250, and 833 kVA DTs in FA cooling mode at SFO for: (a) T_h and (b) T_o.

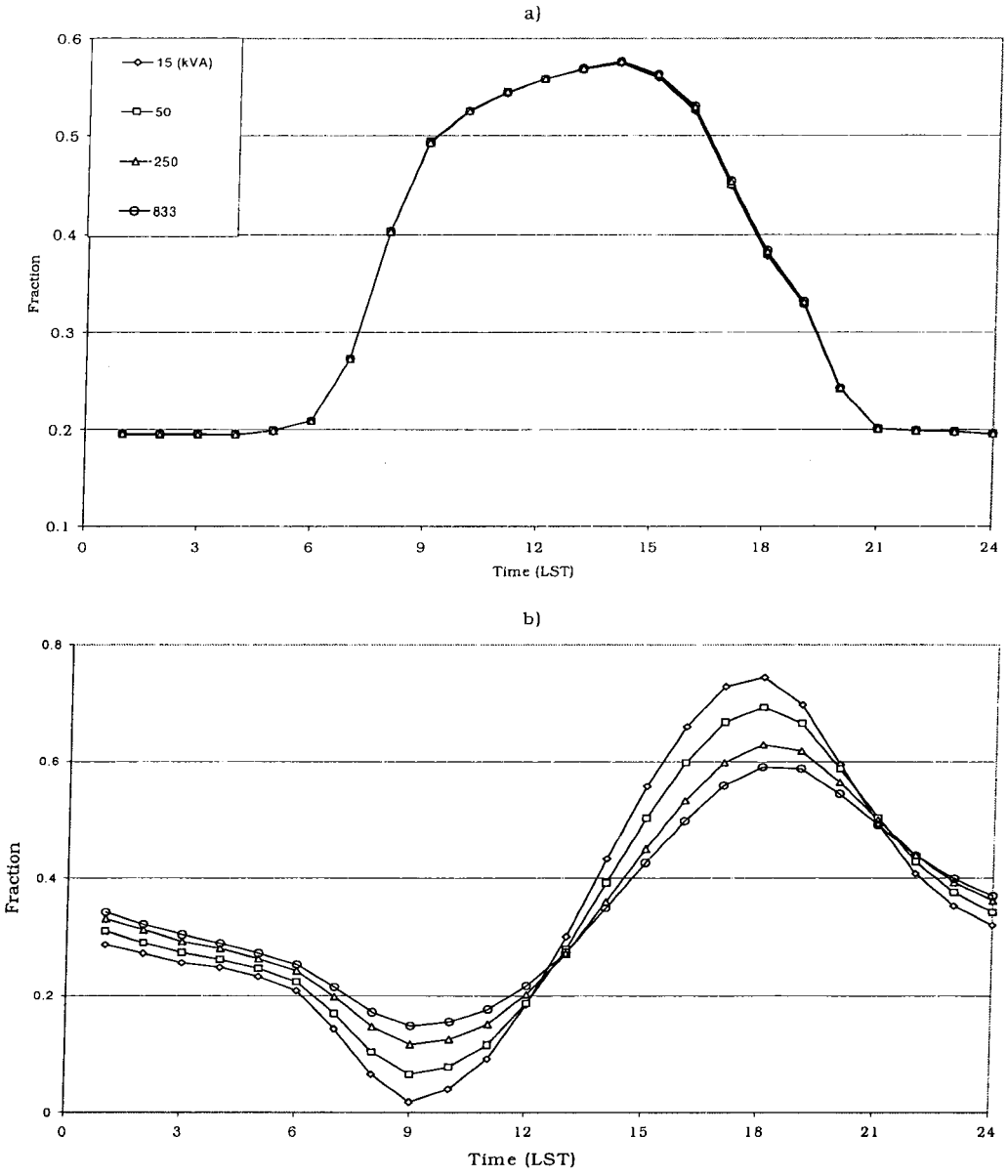

Fig. 19. LBNL03wx average-day fractional heat generation/loss rate for 15, 50, 250, and 833 kVA DTs in FA mode at SFO for: (a) $\dot{Q}_A$ and (b) $\dot{Q}_o$.

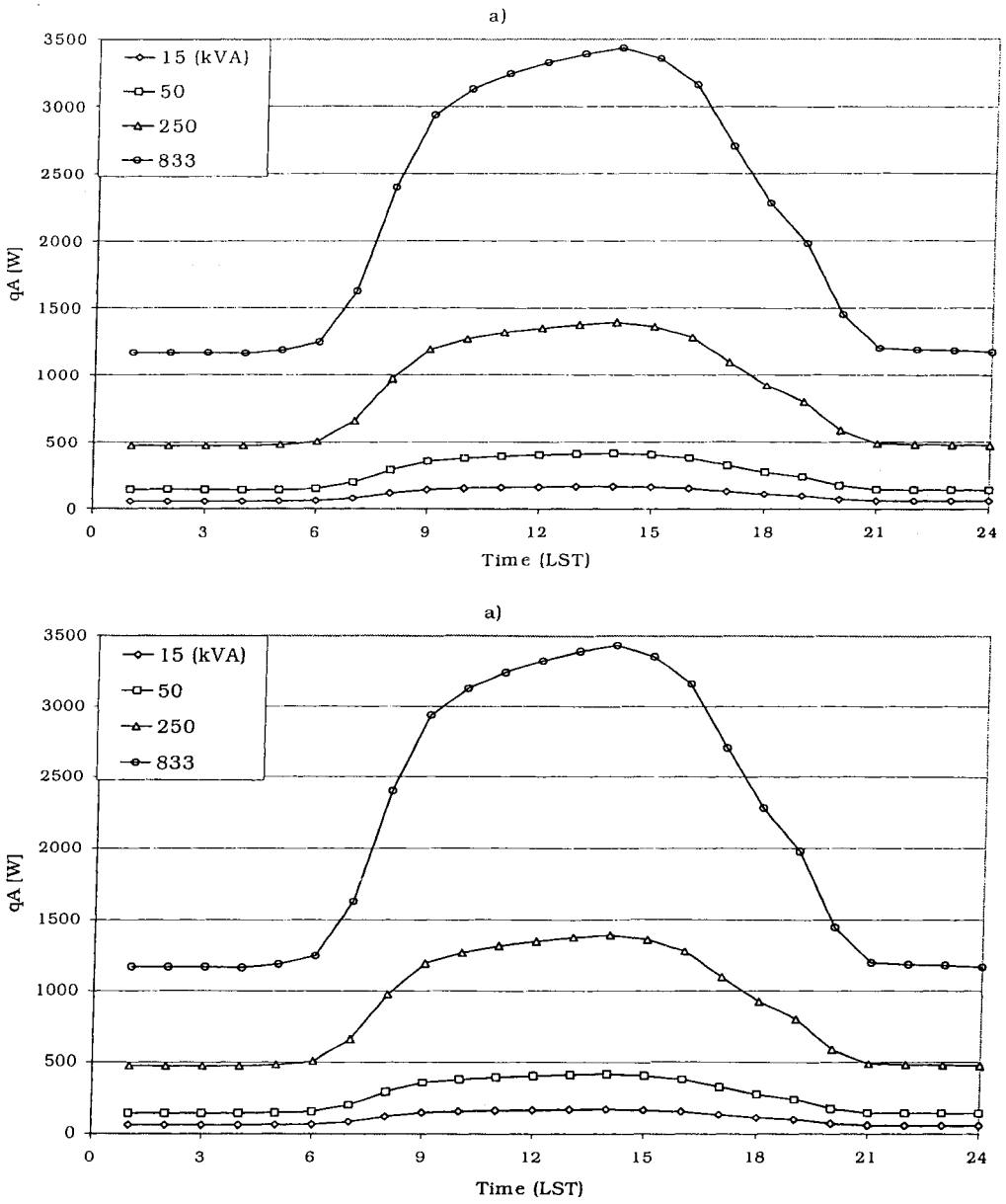

Fig. 20. LBNL03wx average-day un-normalized heat generation/loss rate for 15, 50, 250, and 833 kVA DT in FA cooling mode at SFO for: (a) $\dot{q}_A$ and (b) $\dot{q}_O$.

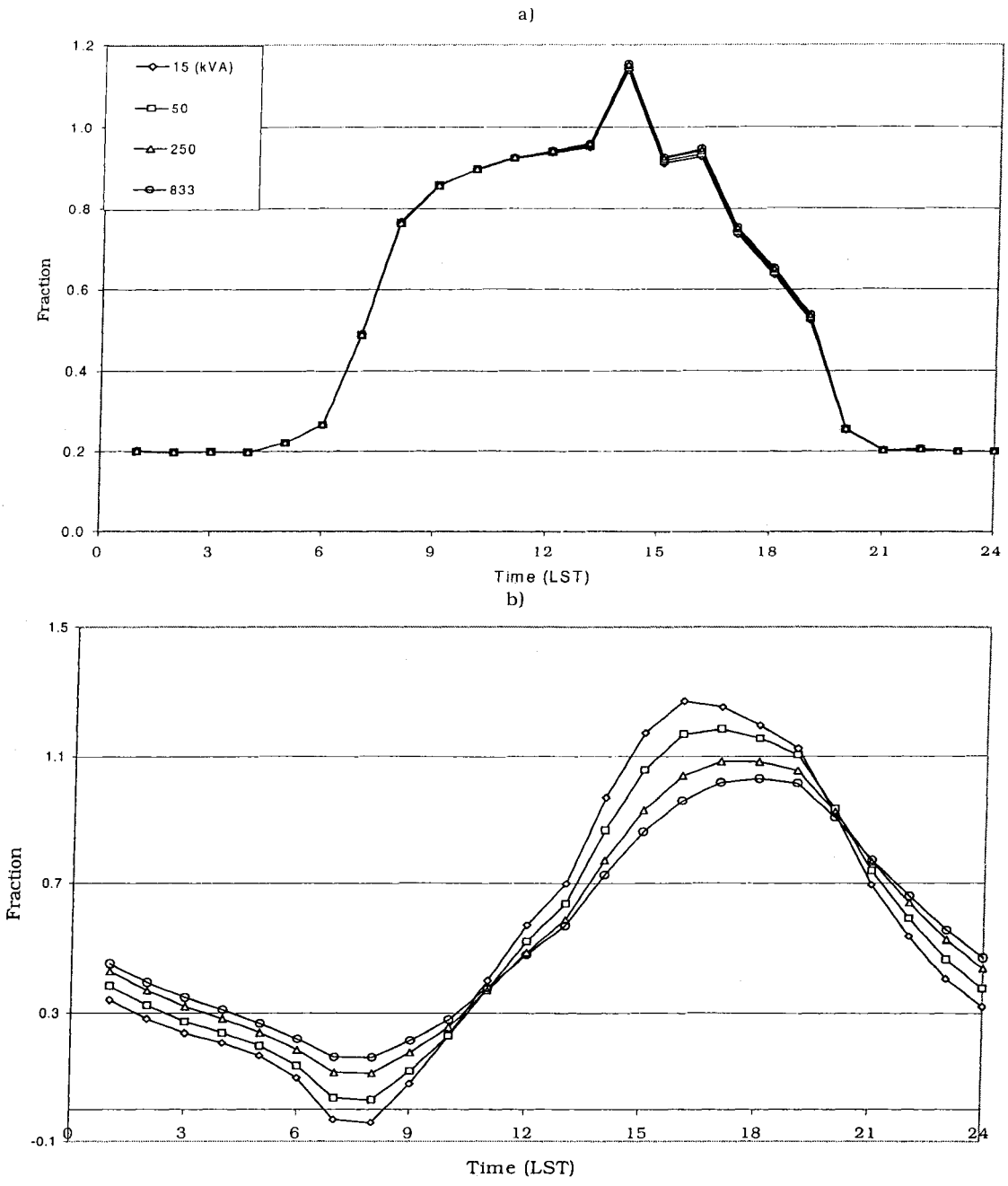

Fig. 21. LBNL03wx hot-spot day fractional heat generation/loss rate for 15, 50, 250, and 833 kVA DTs in FA cooling mode at SFO for: (a) $\dot{Q}_A$ and (b) $\dot{Q}_o$.

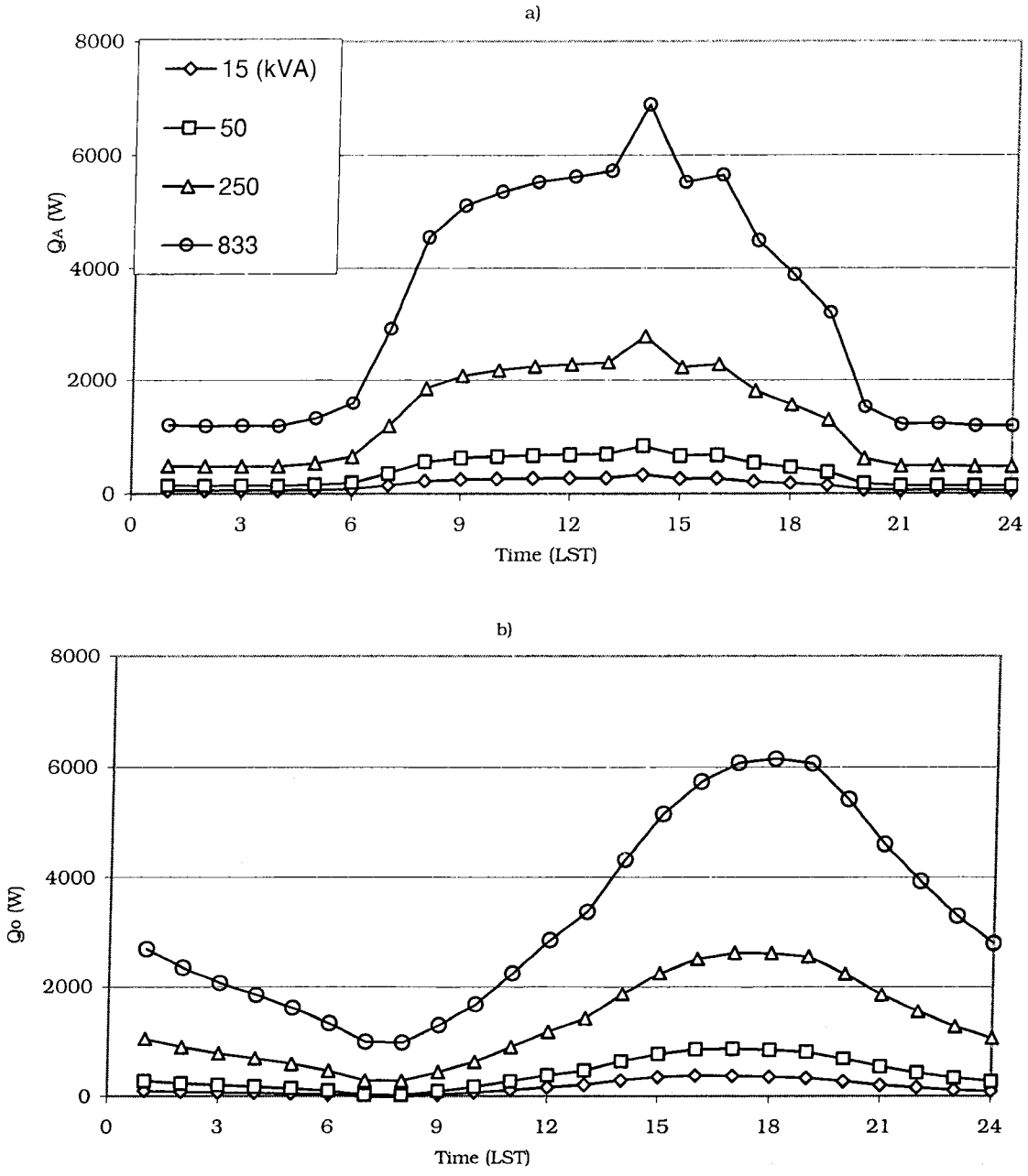

Fig. 22. LBNL03wx hot-spot day un-normalized heat generation/loss rate for 15, 50, 250, and 833 kVA DT in FA cooling mode at SFO for: (a) $\dot{q}_A$ and (b) $\dot{q}_o$

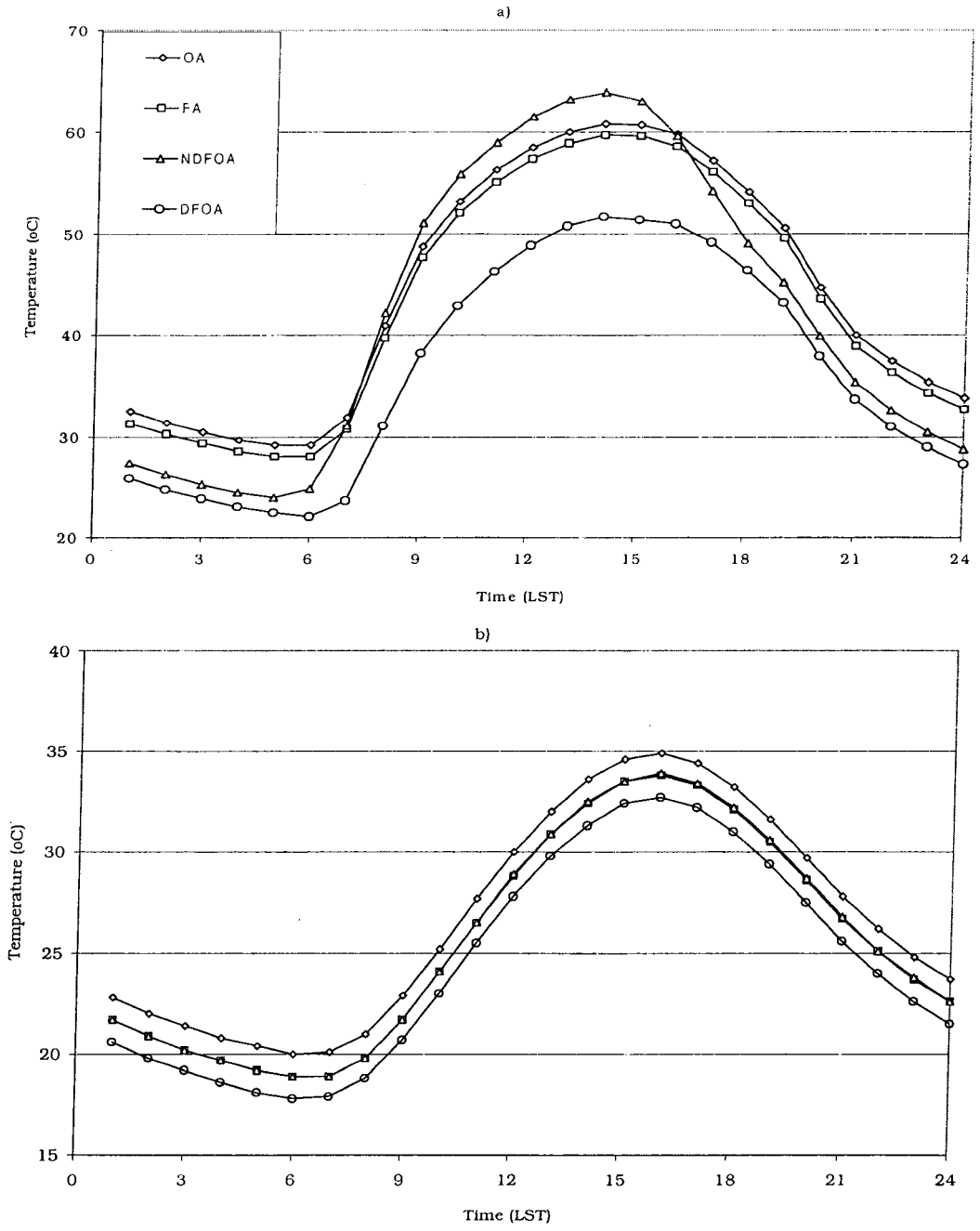

Fig. 23. LBNL03wx average-day 250 kVA DT temperature for OA, FA, NDFOA, and DFOA cooling modes at SFO for: (a) T_h and (b) T_o.

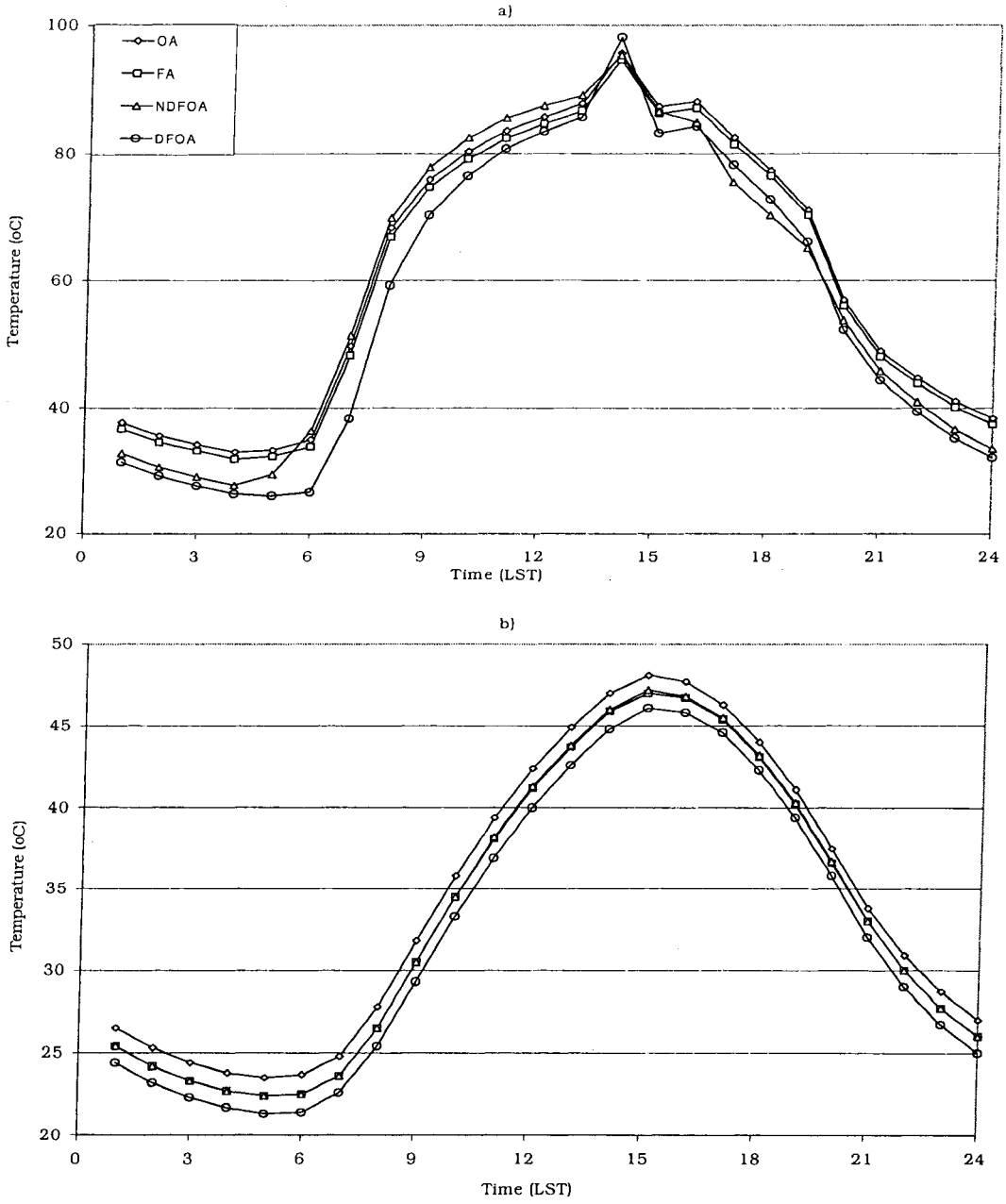

Fig. 24. LBNL03wx hot-spot day 250 kVA DT temperatures for OA, FA, NDFOA, and DFOA cooling modes at SFO for: (a) T_h and (b) T_o.

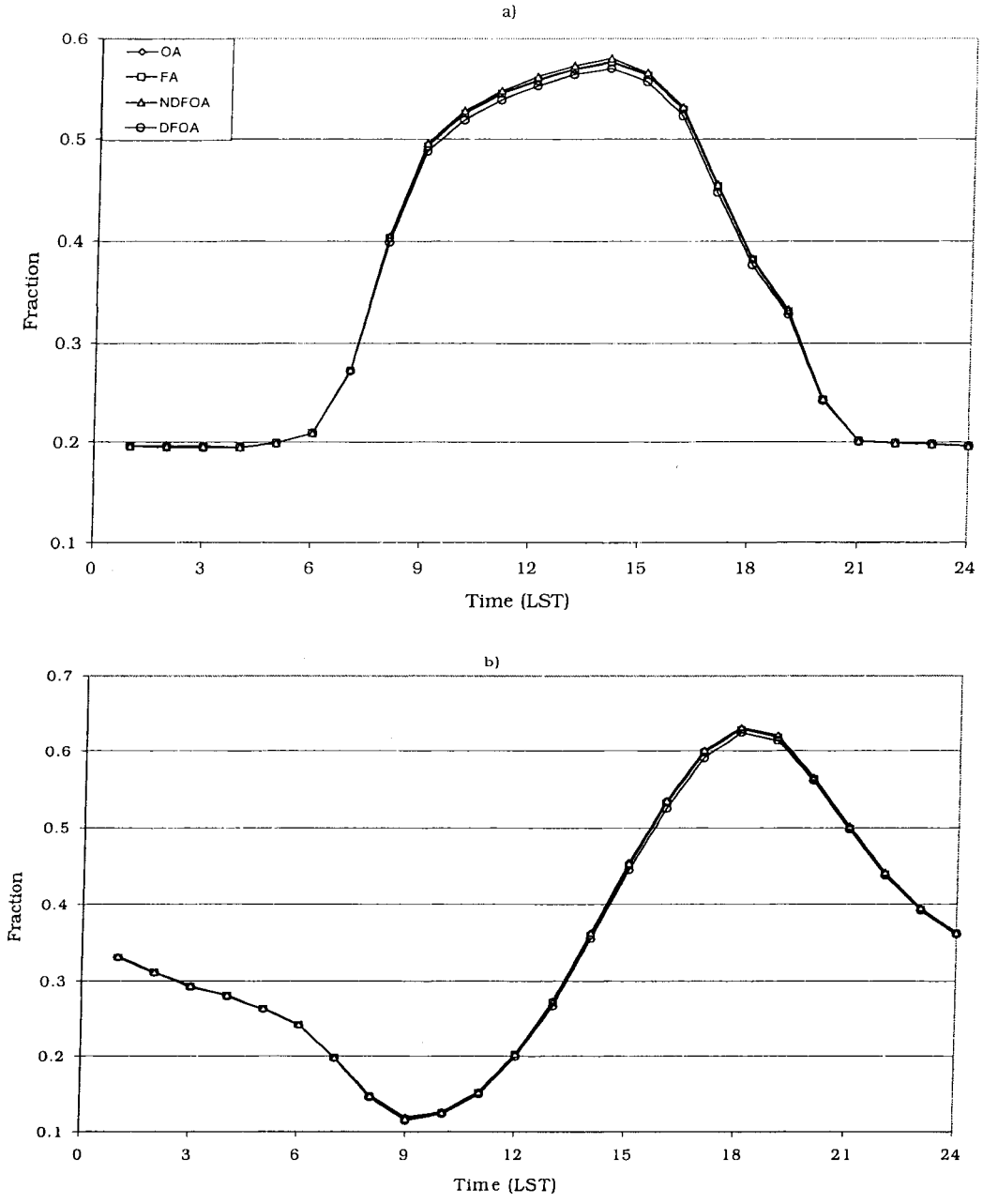

Fig. 25. LBNL03wx average-day 250 kVA DT heat generation/loss rate for OA, FA, NDFOA, and DFOA cooling modes at SFO: (a) $\dot{Q}_A$ and (b) $\dot{Q}_O$.

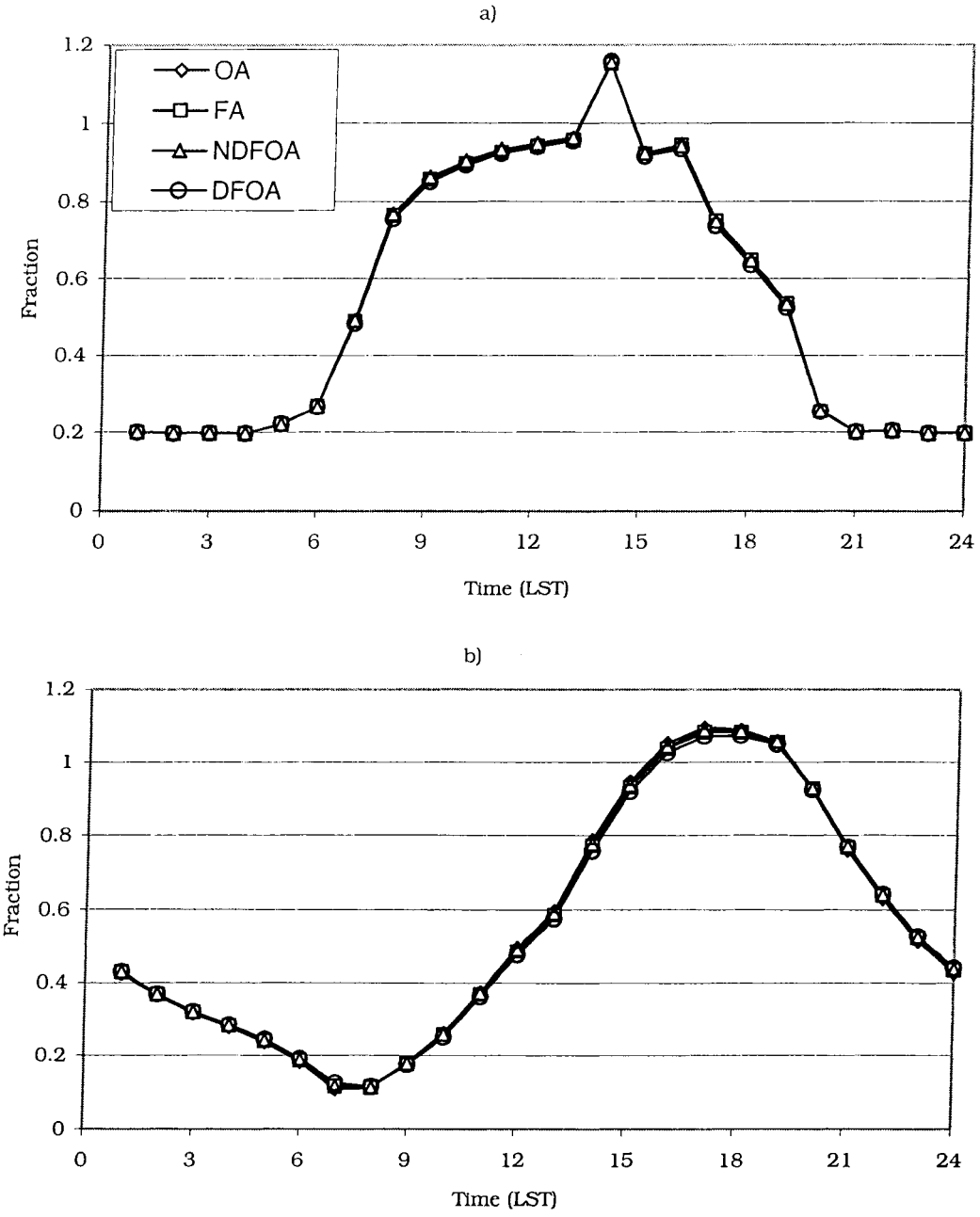

Fig. 26. LBNL03wx hot-spot day 250 kVA DT heat generation/loss rate for OA, FA, NDFOA, and DFOA cooling modes at SFO for: (a) $\dot{Q}_A$ and (b) $\dot{Q}_o$.

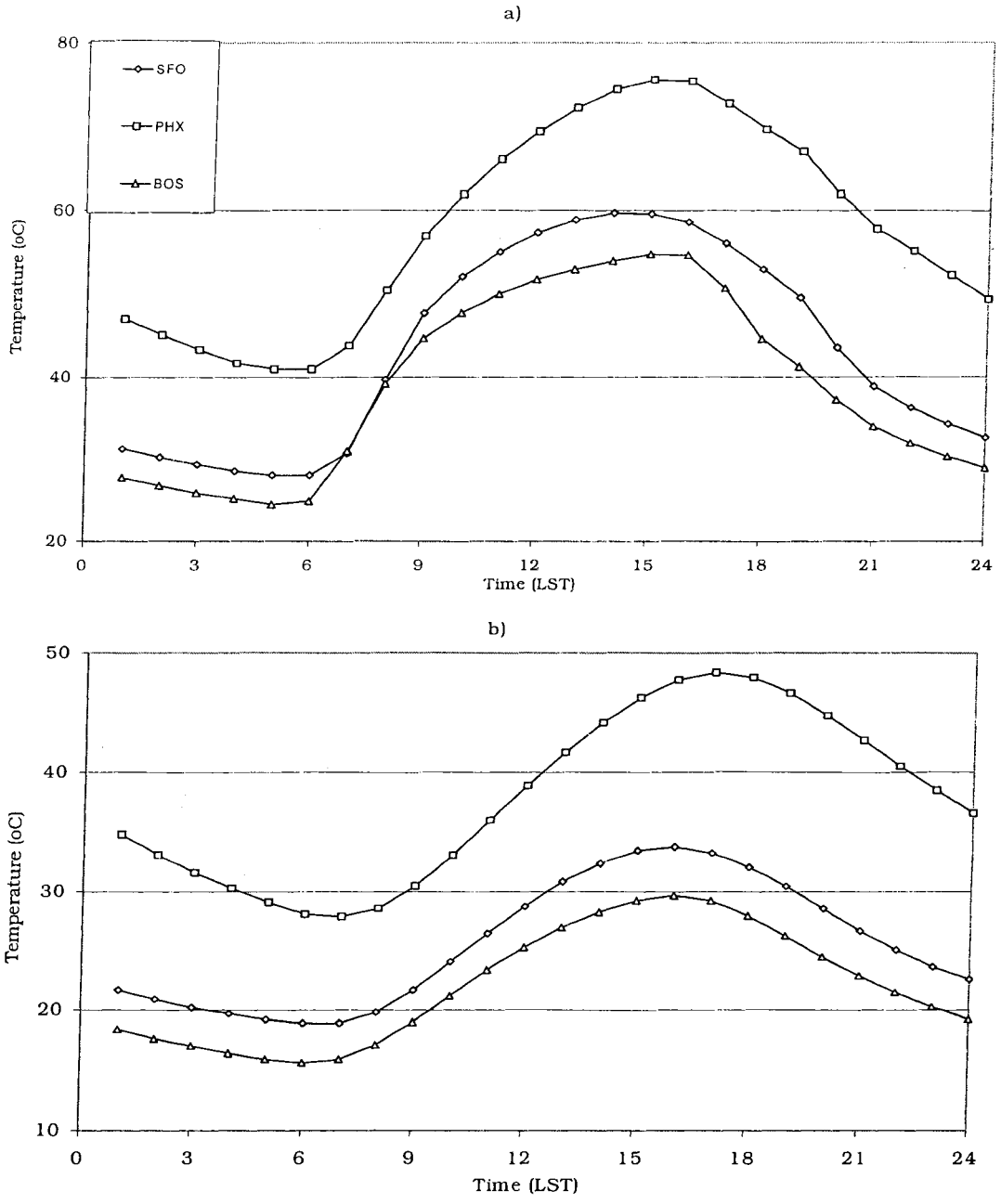

Fig. 27. LBNL03wx average-day temperatures for 250 kVA DT in FA cooling mode at BOS, PHX, and SFO for: (a) T_h and (b) T_o.

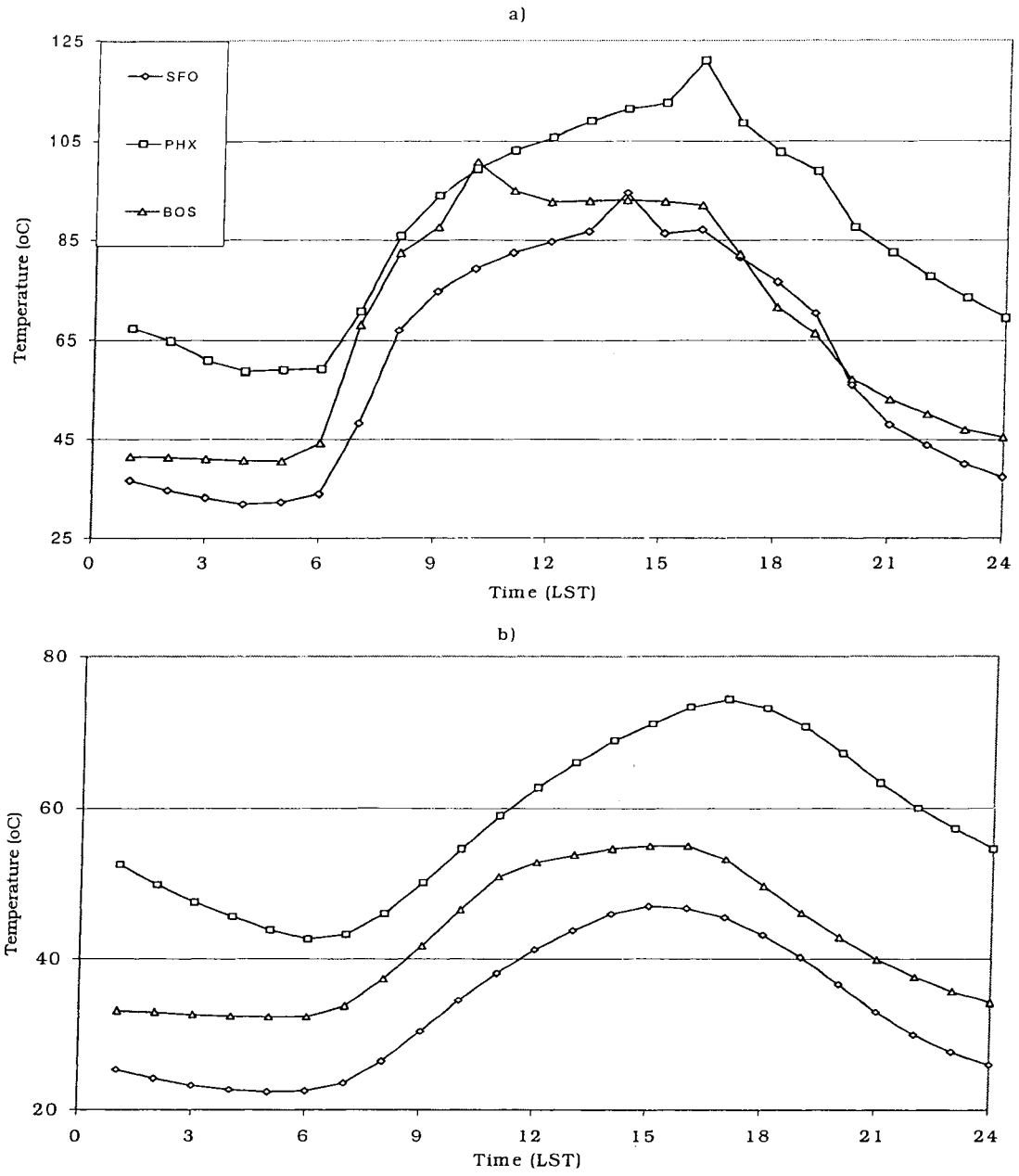

Fig. 28. LBNL03wx hot-spot day temperatures for 250 kVA DT in FA cooling mode at BOS, PHX, and SFO: (a) T_h and (b) T_o.

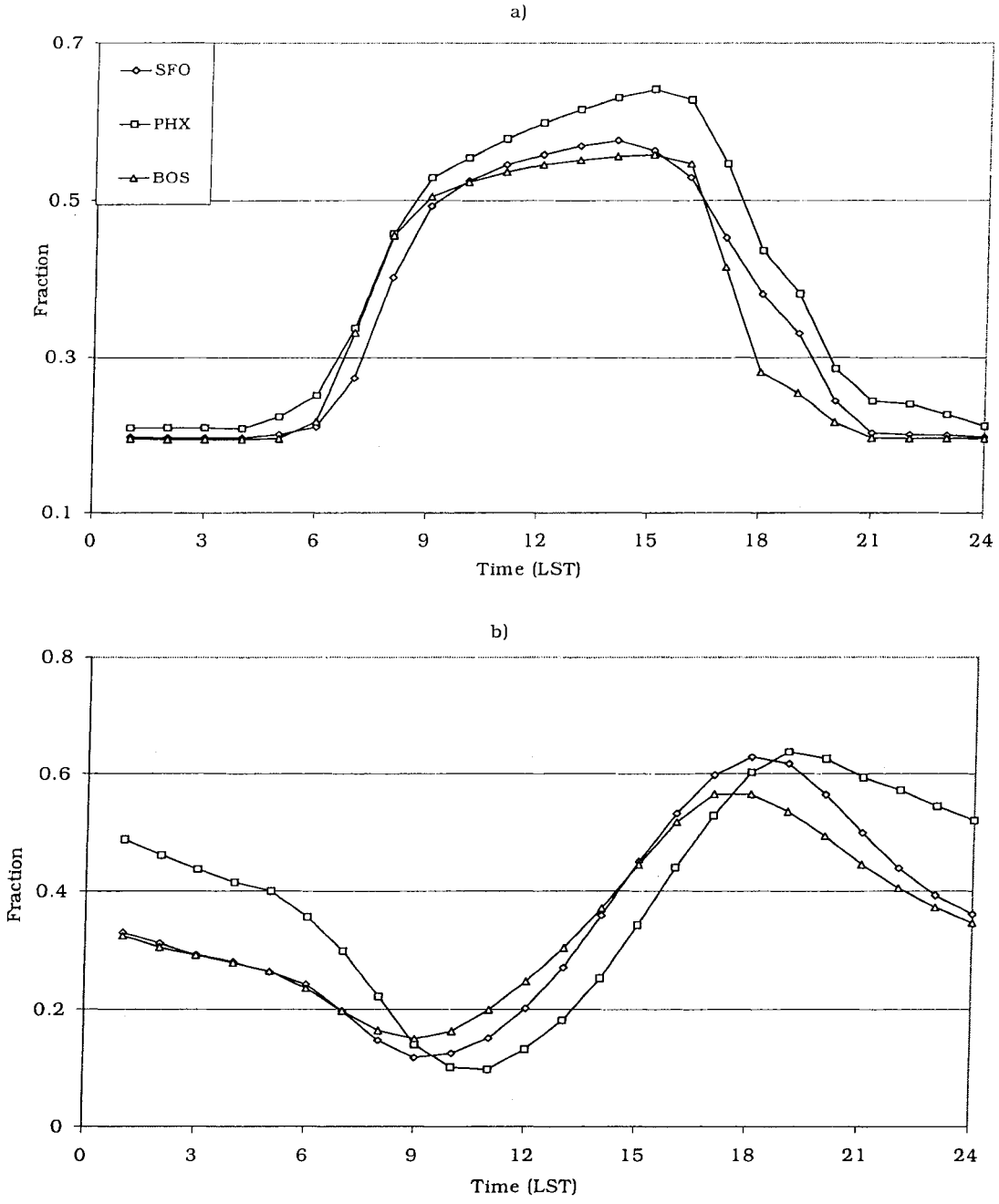

Fig. 29. LBNL03wx average-day heat generation/loss rate for 250 kVA DT in FA cooling mode at BOS, PHX, and SFO for: (a) $\dot{Q}_A$ and (b) $\dot{Q}_o$.

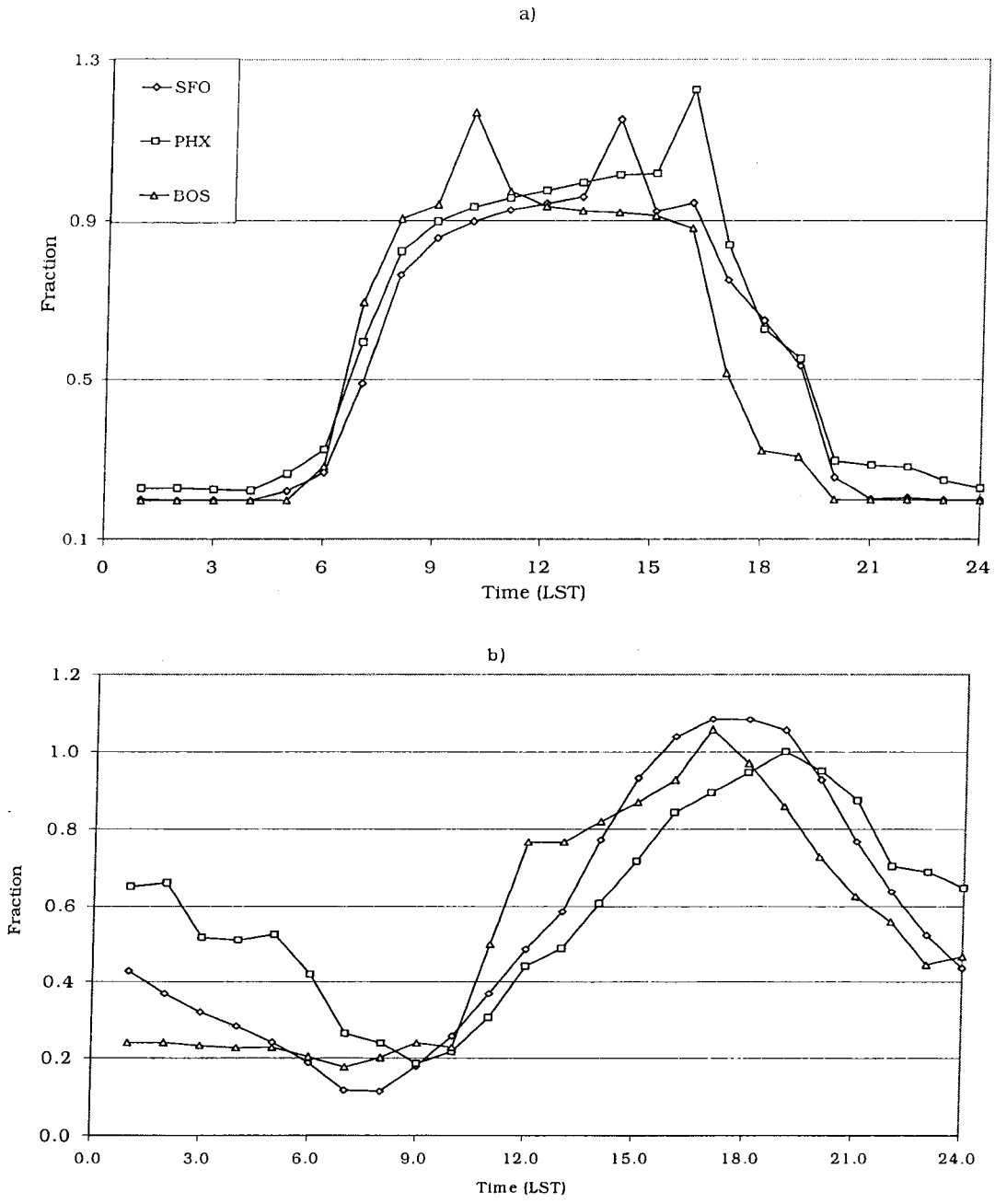

Fig. 30. LBNL03wx hot-spot day heat generation/loss rate for 250 kVA DT in FA cooling mode at BOS, PHX, and SFO for: (a) $\dot{Q}_A$ and (b) $\dot{Q}_o$.

Input Parameter	DT size (kVA)				
	15	50	250	833	28 000
D [m]	0.25	0.33	0.50	0.67	1.58
T_b [°C]	85	85	85	85	75
P_w [W]	231	570	1 907	4 704	51 690
P_e [W]	2.3	5.8	19.4	47.8	0.0
P_s [W]	4.8	11.8	39.3	97	21 078
P_c [W]	55	135	450	1 111	36 986
P_{cx} [W]	55	135	450	1 111	36 986
P_A [W]	293	723	2417	5 960	109 754
$\Delta\tilde{T}_{wa}$ [°C]	65	65	65	65	63
$\tilde{T}_a$ [°C]	20	20	20	20	30
τ [min]	3	3	3	3	5
$(m_c + m_w)$ [kg]	56	139	464	1 145	34 292
m_t [kg]	17	42	139	344	14 243
V_0 [m³]	0.08	0.21	0.69	1.69	18.58

Table 1. Input parameters for five simulations (see Appendix A for symbol definitions).

Constant	Value
Air density, ρ [kg m^{-3}]	1.275
Atmospheric thermal conductivity, λ [W m^{-1} k^{-1}]	2.51 x10^{-2}
DT surface albedo, α [dimensionless]	0.75
Constant in viscosity equation, B [dimensionless]	1.3573x10^{-3}
Constant in viscosity equation, F [dimensionless]	2797.3
Dynamic viscosity coefficient, μ [N s m^{-2}]	1.824x10^{-5}
Winding to hot-spot height ratio, h [dimensionless]	1.0
Resistance-temperature for copper, T_k [°C]	234.5
Rated hot-spot temperature rise, $\Delta\tilde{T}_{ha}$ [°C]	80.0
Rated average winding temperature rise, $\Delta\tilde{T}_{wa}$ [°C]	65.0
Rated top-oil temperature rise, $\Delta\tilde{T}_{Ta}$ [°C]	55.0
Rated bottom-oil temperature, $\Delta\tilde{T}_{Ba}$ [°C]	25.0
Time increment, Δt [h]	1.0

Table 2. Input constants.

Exponent	Oil	Cooling Mode			
		OA	FA	NDFOA	DFOA
x	Duct	0.5	0.5	0.5	1.0
y	Average	0.8	0.9	0.9	1.0
z	Top to bottom	0.5	0.5	1.0	1.0

Table 3. Exponents in temperature-rise and heat-flux calculations for various DT oil locations.

Run No.	Model	Wind	Solar radiation	DT kVA rating	Cooling Mode	Site
1	LBNL03t	calm	No	28 000	FA	Test case
2	LBNL03t	calm	no	250	FA	SFO
3	LBNL03ts	calm	Yes	250	FA	SFO
4	LBNL03tw	windy	no	250	FA	SFO
5	LBNL03wx	windy	Yes	250	FA	SFO
6	LBNL03wx	windy	Yes	15	FA	SFO
7	LBNL03wx	windy	Yes	50	FA	SFO
8	LBNL03wx	windy	Yes	250	FA	SFO
9	LBNL03wx	windy	Yes	833	FA	SFO
10	LBNL03wx	windy	Yes	250	FA	SFO
11	LBNL03wx	windy	Yes	250	OA	SFO
12	LBNL03wx	windy	Yes	250	DFOA	SFO
13	LBNL03wx	windy	Yes	250	NDFOA	SFO
14	LBNL03wx	windy	Yes	250	FA	SFO
15	LBNL03wx	windy	Yes	250	FA	BOS
16	LBNL03wx	windy	Yes	250	FA	PHX

Table 4. Summary of model runs.

	Input		IEEE95				LBNL03t			
t [h]	L [non-dim]	T_a [°C]	T_h [°C]	T_p [°C]	T_d [°C]	T_B [°C]	T_h [°C]	T_p [°C]	T_d [°C]	T_B [°C]
0	0.73	30.0	89.9	74.1	69.6	48.0	89.9	74.1	69.6	48.0
1	0.64	29.5	82.7	69.6	64.0	45.0	82.7	69.6	64.0	45.0
2	0.62	29.2	77.9	65.4	60.5	42.4	77.9	65.4	60.5	42.4
3	0.61	29.0	74.5	62.5	58.1	40.6	74.5	62.5	58.1	40.6
4	0.59	28.7	71.9	60.4	56.2	39.3	71.9	60.4	56.2	39.3
5	0.58	28.5	69.7	58.6	54.6	38.2	69.7	58.6	54.6	38.2
6	0.56	28.2	67.8	57.2	53.2	37.3	67.8	57.2	53.2	37.3
7	0.62	29.8	68.7	56.6	54.9	37.7	68.7	56.6	54.9	37.7
8	0.71	31.8	73.7	59.3	59.3	39.7	73.7	59.3	59.3	39.7
9	0.79	33.9	82.4	65.2	65.2	42.9	82.4	65.2	65.2	42.9
10	0.88	35.9	92.3	72.2	72.2	47.1	92.3	72.2	72.2	47.1
11	0.93	37.1	100.4	78.4	78.4	51.3	100.4	78.4	78.4	51.3
12	0.98	38.4	108.0	84.3	84.3	55.4	108.0	84.3	84.3	55.4
13	1.03	39.6	115.7	90.1	90.1	59.5	115.7	90.1	90.1	59.5
14	1.07	40.0	122.3	95.3	95.3	63.1	122.3	95.3	95.3	63.1
15	1.10	40.0	127.7	99.5	99.5	66.1	127.7	99.5	99.5	66.1
16	1.10	39.6	130.0	101.7	101.7	68.0	130.0	101.7	101.7	68.0
17	1.07	38.2	128.4	101.1	101.1	68.2	128.4	101.1	101.1	68.2
18	1.04	36.8	125.7	99.6	98.9	66.9	125.7	99.6	98.9	66.9
19	0.99	35.4	121.0	96.7	94.8	64.6	121.0	96.7	94.8	64.6
20	0.93	33.9	115.1	92.6	89.8	61.3	115.1	92.6	89.8	61.3
21	0.88	32.5	108.6	87.9	84.4	57.7	108.6	87.9	84.4	57.7
22	0.83	31.7	102.1	83.1	79.2	54.3	102.1	83.1	79.2	54.3
23	0.78	30.8	95.9	78.5	74.3	51.1	95.9	78.5	74.3	51.1
24	0.73	30.0	89.9	74.1	69.6	48.0	89.9	74.1	69.6	48.0

Table 5. IEEE95 and LBNL03t test-case hourly input and output for a 28 000 kVA DT in FA cooling mode.

		LBNL03ts – IEEE95		LBNL03tw – IEEE95		LBNL03wx – IEEE95	
Site	DT size (kVA)	Average	Hot-spot	Average	Hot-spot	Average	Hot-spot
SFO	15	13.0	16.5	-7.0	-13.2	-1.1	-6.4
	50	9.4	12.2	-6.5	-11.7	-0.8	-4.2
	250	6.1	8.1	-4.9	-8.2	-0.3	-2.2
	833	4.5	6.0	-3.7	-6.0	-0.1	-1.2
	28 000	0.7	0.8	-0.5	-1.3	0.1	-0.2
BOS	15	10.7	16.4	-8.4	-9.4	-3.0	-0.4
	50	7.9	12.2	-7.4	-8.0	-2.3	-1.4
	250	5.2	8.2	-5.6	-9.0	-1.5	-1.6
	833	3.9	6.1	-4.2	-12.7	-1.9	-1.8
	28 000	0.6	0.6	-0.5	-0.4	0.1	0.2
PHX	15	14.7	7.7	-7.0	-15.8	1.4	-7.1
	50	10.7	12.7	-5.9	-12.6	1.6	-4.9
	250	6.9	8.5	-4.3	-8.8	1.4	-2.7
	833	5.1	6.3	-3.2	-6.5	1.2	-1.5
	28 000	0.7	0.9	-0.4	-0.9	0.3	-0.1

a)

		LBNL03ts – IEEE95		LBNL03tw – IEEE95		LBNL03wx – IEEE95	
Site	DT size (kVA)	Average	Hot-spot	Average	Hot-spot	Average	Hot-spot
SFO	15	11.6	16.2	-9.6	-16.6	-2.8	-7.7
	50	8.6	12.0	-8.1	-13.5	-2.1	-5.9
	250	5.8	8.0	-5.6	-17.9	-1.1	-4.2
	833	4.3	5.9	-4.2	-7.5	-0.6	-2.7
	28 000	0.7	0.9	-0.6	-1.2	0.1	-0.3
BOS	15	10.5	16.4	-9.9	-17.6	-4.2	-10.3
	50	7.6	12.1	-8.1	-15.6	-3.1	-8.5
	250	5.1	8.1	-5.9	-8.7	-1.9	-6.3
	833	3.8	6.0	-4.4	-9.5	-1.3	-5.1
	28 000	0.4	0.7	-0.6	-0.5	-0.1	0.1
PHX	15	13.3	16.9	-8.3	-15.6	0.9	-7.4
	50	9.8	12.6	-6.7	-12.4	0.4	-5.2
	250	6.5	8.4	-4.6	-8.6	0.7	-2.5
	833	4.7	6.3	-3.4	-6.3	0.8	-1.3
	28 000	0.7	0.8	-0.4	-0.9	0.3	-0.1

b)

Table 6. Peak-hour average-day and hot-spot day DT model differences (^{o}C) due to various weather effect for: a) hot-spot T_h and b) oil T_o.

Site	DT Size (kVA)	IEEE95	LBNL03ts	LBNL03tw	LBNL03wx
SFO	15	24.9	142.2	7.6	18.8
	50	24.9	89.7	8.7	20.2
	250	24.9	58.3	11.4	22.0
	833	24.9	46.6	15.8	23.3
	28 000	53.3	57.9	46.7	52.9
BOS	15	62.1	310.1	17.0	40.6
	50	62.1	203.5	20.4	45.7
	250	62.1	137.2	27.8	52.2
	833	62.1	111.7	34.2	56.3
	28 000	138.8	150.0	127.0	137.1
PHX	15	321.5	1 712.7	98.4	292.4
	50	321.5	1 109.9	123.0	310.0
	250	321.5	737.5	164.6	329.0
	833	321.5	595.4	196.7	338.6
	28 000	656.4	712.0	613.0	664.0

a)

Site	Size (kVA)	(LBNL03ts–IEEE95) /IEEE95 [%]	(LBNL03tw–IEEE95) /IEEE95 [%]	(LBNL03tsw–IEEE95) /IEEE95 [%]
SFO	15	471	-69	-24
	50	260	-65	-19
	250	134	-54	-12
	833	87	-37	-6
	28 000	9	-12	-1
BOS	15	399	-73	-35
	50	228	-67	-26
	250	121	-55	-16
	833	80	-45	-9
	28 000	8	-9	-1
PHX	15	433	-69	-9
	50	245	-62	-4
	250	129	-49	2
	833	85	-39	5
	28 000	9	-7	1

b)

Table 7. DT equivalent aging parameter E_A (h): (a) from four models and (b) as model differences (% of IEEE95).